EIT InnoEnergy Master's in Energy Storage

Grading and Quality Control of Zinc-Ion Battery Cells

Testing and Developing a Quality Control System to be Implemented in the Manufacturing and Formation of Zinc-Ion Battery Cells

---

Miguel Lacerda Alegre Abranches Farias

Master's Thesis 2023

The thesis is written as part of a collaborative joint degree programme called Master's Programme in Energy Storage (EIT InnoEnergy).

Aalto University is responsible for the implementation of the programme along with Politecnico di Torino (PoliTo) and EIT InnoEnergy, a knowledge and innovation community of the European Institute of Innovation and Technology.

The thesis is supervised by both partner universities.

Politecnico di Torino

Aalto University

Copyright ©2022 Miguel Lacerda Alegre Abranches Farias

Aalto-yliopisto
Aalto-universitetet
Aalto University

Author Miguel Lacerda Alegre Abranches Farias

Title of thesis Grading and Quality Control of Zinc-Ion Battery Cells

Programme EIT InnoEnergy Master's in Energy Storage

Thesis supervisor Tanja Kallio (Aalto University); Davide Papurello (Politecnico di Torino)

Thesis advisor(s) Dr Mylad Chamoun, PhD

Collaborative partner Enerpoly AB

Date 07.07.2023 **Number of pages** 81 **Language** English

Abstract

This paper presents the analysis and results developed during a master thesis internship with the Swedish company Enerpoly AB. The objective of the thesis was to assess and establish a grading and quality control system for the zinc-ion battery cells manufactured by the company. For this purpose, several pouch cells were assembled and submitted to formation cycles, self-discharge, and cycle life tests. While from an initial study, analysing and relating the formation cycle parameters, it was concluded that 2 formation cycles are sufficient for a stable operation of the cell, no reliable outcomes were reached from the self-discharge tests due to a problem in the cycler. Lastly, concerning the cycle life tests, even though no strong correlations were encountered between the formation cycle parameters and the good or bad performances of the cells, significant conclusions were drawn from the data analysis. On one hand, some of the cells assembled presented very stable behaviours throughout the cycling protocol, only fading capacity because of external factors such as electrolyte drying or coating delamination. On the other hand, malfunctioning cells, discarded from the analysis, were always identified by either a fast rise of their internal resistance or a low initial gravimetric capacity. For these reasons, it was concluded that the grading and quality control system suggested to be implemented in the manufacturing process should consist of 2 independent stages: quality control checks on the dry cell – such as checking case sealing, absence of short circuits, and the coating quality – would ensure that no external factors influence the cell's performance; and quality control checks after electrolyte injection – including internal resistance and capacity measurements before and after formation – guarantee that malfunctioning cells can be discarded and recycled before integrating the battery pack.

Keywords Zinc-ion battery, Cell grading, Quality control, Cycling life, Cell formation, Cell self-discharge.

Table of contents

Tables 7
Figures 7
Abbreviations 9
Acknowledgements 11
1 Introduction 12
2 State-of-the-art Review 15
2.1 Zinc-Ion Battery System 15
2.2 Battery Cell Specifications 18
2.3 Battery Grading 19
2.3.1 The Importance of Battery Grading 19
2.3.2 Tests performed for Battery Grading 21
2.3.3 Capacity Test 21
2.3.4 Open Circuit Voltage (OCV) Test 22
2.3.5 Internal Resistance – Pulse Power Test 24
2.3.6 Internal Resistance – Electrochemical Impedance Spectroscopy (EIS) Test 26
2.3.7 Self-Discharge Test 27
2.3.8 Cycle Life Test 28
2.3.9 Insulation Test 31
3 Pouch Cell Assembly 32
4 Primary Cell Testing 34
4.1 Methodology and Protocol 34
4.2 Results and Discussion 37
5 Study of the 2-Plateau Self-Discharge Curve 39
5.1 Self-Discharge with Different Number of Formation Cycles Testing 39
5.1.1 Methodology and Protocol 39
5.1.2 Correlations between Formation Cycle Parameters 40
5.1.3 Self-Discharge Curves Study 47
5.2 Self-Discharge with Different Cathodic Current Collector 48
5.3 Self-Discharge due to Current Leakage Problem from the Cycler 49
6 Self-Discharge Tests 51
6.1 Methodology and Protocol 51
6.2 2-Week Self-Discharge Tests 52
6.3 3-Day Self-Discharge Tests 53

7 Cycle Life Tests 55
7.1 Methodology and Protocol 55
7.2 Cycle Life Data Analysis Method 57
7.3 Room Temperature Dataset 58
7.4 25°C Dataset 61
7.5 5°C Dataset 64
7.6 Analysis Combining the Different Datasets 65
7.7 Slow Cycle Life Tests 67
7.8 Conclusions from the Cycle Life Tests 70
8 Summary and Conclusions 72
9 Future Research 74
References 75

Tables

Table 1– Experimental procedure for the measurement of OCV as a function of SoC 23
Table 2 – Cycler protocol for the different parts of the primary cell testing. 35
Table 3 – Formation cycle parameters divided into 3 categories. 40
Table 4 – Formation cycle parameters analysed in the correlation study. 41
Table 5– Formation cycle parameters evaluated in future studies. 46
Table 6 – Protocol used for the self-discharge tests. 51
Table 7 – Protocol used for the cycle life tests. 55
Table 8 – Protocol used for the slow cycle life tests. 67

Figures

Figure 1– Representative charge-discharge curve of Zn/MnO_2 batteries 18
Figure 2 – Correlation between capacity and temperature for a lithium-ion battery. 22
Figure 3 – SOC-OCV relation at different temperatures for a lithium-ion battery.24
Figure 4 – Schematic of the voltage response to a square-wave current for a pulse power test....25
Figure 5 – Internal resistance as a function of temperature for several different chemistries....25
Figure 6 – General Nyquist Plot 26
Figure 7 – Self-discharge curves for a lithium-ion cell for different temperatures (a), in logarithmic scale (b) and as a function of $time^{1/2}$ (c) 28
Figure 8 – Influence of temperature on the cycle life of a lithium-ion battery....29
Figure 9 – Effect of C-rate on the cycle life of a LCO lithium-ion battery....29
Figure 10 – Cycle performance as a function of the depth of discharge for a rechargeable zinc-manganese dioxide AAA cell 30
Figure 11 – LCO lithium-ion cell capacity as a function of the number of cycles for different values of charging cut-off voltage 30
Figure 12– Pouch cell assembly steps: (a) current collector side of the cathode; (b) active side of the cathode; (c) and (d) sides of the anode with and without the negative terminal, respectively; (e) and (f) anode and cathode side, respectively, of both electrodes joint with the separator in the middle; (g) both electrodes and separator in the pouch bag with 3 of its sides sealed; (h) electrolyte filling; (i) and (j) final pouch cell – anode and cathode side, respectively 33
Figure 13 – Pictures taken in the lab of: (a) and (b) current collector and active side of the cathode, respectively; (c) and (d) anode sides with and without the terminal, respectively; (e) and (f) cathode and anode side, respectively, of the ensemble constituted by both electrodes, separator, and cell case; (g) and (h) cathode and anode side, respectively, of the final pouch cell 33
Figure 14 – Cycling Curves for Cells P2231 and P2232 37
Figure 15 – (a) Self-Discharge curve for cells P2231 and P2232; (b) Cycle life cycling curve for cell P2231.... 38

Figure 16 – Formation Cycles Cycling Curves for the 8 tested cells.....39
Figure 17 – Charge and discharge curves of cell P2257 for each formation cycle.. 40
Figure 18 – Correlations between the parameters related to the 1st formation cycle. 42
Figure 19 – Correlations between the parameters related to the 2nd formation cycle. 43
Figure 20 – Correlations between the parameters related to the 3rd formation cycle 43
Figure 21 – Linear Relation between the average and the median discharge voltage for each cycle..... 44
Figure 22 – Correlations between the formation cycles parameters using every data point..... 44
Figure 23– Correlation between the formation cycles parameters and capacity retention 45
Figure 24 – Formation cycle parameters as a function of the cycle number 47
Figure 25– Self-discharge curve for the 8 cells formed with different number of formation cycles.....47
Figure 26 – Self-discharge curves for both cells using stainless steel as a cathodic current collector..... 49
Figure 27 – Self-discharge curves for 9 cells as a means of testing the cycler 50
Figure 28 – 2-week self-discharge curves obtained from the non-faulty cycler 52
Figure 29 – 3-day self-discharge curves.....53
Figure 30 – Cycle life data analysis method. 58
Figure 31 – Discharge DCIR and capacity as a function of cycle number for the room temperature dataset 59
Figure 32 – Capacity retention as a function of cycle number for the room temperature dataset.....59
Figure 33 – Correlation matrix for the room temperature dataset..... 60
Figure 34 – Good (positive value) or bad (negative value) behaviour of the cell as a function of the 1st formation cycle voltage drop after charging for the 3 chosen thresholds. 61
Figure 35 - Discharge DCIR and capacity as a function of cycle number for the 25°C dataset.....62
Figure 36 - Capacity retention as a function of cycle number for the 25°C dataset62
Figure 37 - Correlation matrix for the 25°C dataset.....63
Figure 38 - Good (positive value) or bad (negative value) behaviour of the cell as a function of the 1st formation cycle DCIR for the 3 chosen thresholds.....63
Figure 39 - Discharge DCIR and capacity as a function of cycle number for the 5°C dataset..... 64
Figure 40 - Capacity retention as a function of cycle number for the 5°C dataset..65
Figure 41 - Correlation matrix for the 5°C dataset 65
Figure 42 – Correlation matrix for all datasets combined 66
Figure 43 – Correlation matrix for the combination of the 25°C and 5°C datasets and for the combination of the room temperature and 25°C datasets..... 66
Figure 44 - Discharge capacity and DCIR as a function of the cycle number for both cells 68
Figure 45 – Capacity retention as a function of cycle number and cycling curve of cell P2399..... 69

Figure 46 – Post-mortem analysis of cell P2399 – the cathodic coating is delaminated from the current collector and stuck into the separator. 70

Abbreviations

Zn	Zinc
Mn	Manganese
MnO_2	Manganese Dioxide
SHE	Standard Hydrogen Electrode
Li	Lithium
Zn^{2+}	Zinc Ion
e^-	Electron
ZnO	Zinc Oxide
$ZnSO_4$	Zinc Sulfate
MnO_x	Manganese Oxides
H^+	Proton
ZHS	Zinc Hydroxide Sulfate
$Zn_4(OH)_6(SO_4)$	Zinc Hydroxide Sulfate
MnOOH	Manganese Oxide Hydroxide
SCE	Saturated Calomel Electrode
$ZnMn_2O_4$	Zinc-Manganese Spinel
Ar	Argon
Mn_3O_4	Manganese (II, III) Oxide
OH^-	Hydroxide Ion
SO_4^{2-}	Sulfate Ion
PE	Polyethylene
EMD	Manganese Dioxide Powder
$MnSO_4$	Manganese Sulfate
V	Voltage
OCV	Open Circuit Voltage
C	Capacity
t_o	Initial Time
$t_{cut\text{-}off}$	Cut-off Time
I	Current
$\Delta t_{Discharge}$	Discharge Duration
R_{eq}	Equivalent Resistance
SoC	State-of-charge
U_{limit}	Cut-off Voltage
EIS	Electrochemical Impedance Spectroscopy
HPPC	Hybrid Pulse Power Characterisation
DC	Direct Current
iR	Internal Resistance
R_o	Ohmic Resistance
R_{CT}	Charge Transfer Resistance
R_P	Polarisation Resistance

ΔV	Voltage Drop
AC	Alternate Current
$Z(w)$	Impedance
w	Frequency
$1/RC$	Characteristic Frequency
Δt	Time Interval
DoD	Depth of Discharge
m	Mass
NFC	Number of Formation Cycles
CC	Constant Current
CV	Constant Voltage
DCIR	Direct Current Internal Resistance
R^2	Coefficient of Determination

Acknowledgements

I am very grateful for the opportunity by Enerpoly AB to conduct and develop the tests and research that lead to this thesis, using their facilities and resources during the internship period - from March to July 2023. I would like to thank the whole team for their continuous support and help throughout the internship, but especially Mylad Chamoun and Hsin-Yi Wang for always finding time to discuss my findings and future steps.

Furthermore, I want to thank my supervisor at Aalto University, Tanja Kallio, and my supervisor at Politecnico di Torino, Davide Papurello, for their constructive insight and feedback that helped me achieve a better outcome. Moreover, to Professors Annukka Santasalo-Aarnio and Silvia Bodoardo, coordinators of the master's programme, for all the assistance provided in these two years.

Lastly, I would like to extend my gratitude to my family and friends for their unconditional support through these two academic years.

1 Introduction

Currently, as the world faces and increasing demand for electrical energy storage, lithium-ion batteries are the most popular storage option, controlling more than 90% of the global grid market [1]. However, this battery chemistry presents several safety and material drawbacks. While their flammability and toxic nature create important security and safety concerns [2], the materials that constitute them (mainly lithium, Li, cobalt, Co, and nickel, Ni) are becoming scarce and expensive, causing the rise of the cost of these systems [3]. Furthermore, the prices related to these materials are not only becoming high, but also very volatile, making lithium-ion battery manufacturers and companies unsure on how future trends will influence their businesses [4].

Since presently China controls the lithium-ion battery production market, not only being estimated that, in 2022, 77% of all worldwide capacity was produced there but also hosting 6 of the 10 larger battery manufacturers [5], Europe is specially suffering from these high prices, being assessed that the cost of a battery pack is 33% higher than in Asia [6]. These circumstances were only aggravated by the Covid-19 pandemic and the current Ukraine war, making lithium the world's most volatile commodity for the past 2 years [7].

Due to all these reasons, in the recent years many alternative rechargeable battery chemistries have appeared in the market with the intent of replacing lithium-ion batteries for certain applications. Zinc-ion batteries are considered one of the best options, presenting lower cost, high safety, and easier recyclability [8]. Among them, zinc-manganese (Zn/MnO_2) batteries appear as a promising technology, due to manganese's low toxicity and combustibility, high storage capacity, and high ionic conductivity [9].

On one hand, zinc possesses a high theoretical capacity (820 mAh/g and 5864 mAh/cm^3 [10]) and low standard electrode potential (-0.76 V vs SHE [11]). Moreover, studies have shown the good stability of zinc anodes in aqueous (alkaline, neutral, or weakly acidic) electrolytes and proven the effectiveness of the electrodeposition process on its surface, reaching coulombic efficiencies above 90% [12].

On the other hand, due to their water-based electrolytes, which are also highly ionic-conductive [13], these batteries present an intrinsic nonflammability and low toxicity, leading to better safety characteristics compared with the lithium-ion chemistry.

Lastly, due to the large industrial availability of both zinc – estimated to have reached a total worldwide production of approximately 100 times higher than lithium in 2022 [14], [15] – and manganese, these batteries are not resource restricted [16], which ensures reliability and scalability to their manufacturers. Furthermore, as a consequence of their high accessibility, when compared with lithium, cobalt or nickel, the materials that compose aqueous zinc-ion batteries usually present much lower and less volatile prices, resulting in a cheaper manufacturing cost [9].

Nevertheless, some challenges still exist in the research and manufacturing of zinc-ion batteries, such as the fully comprehension of the cathodic reaction mechanisms [17], the deteriorating effect of cathode and anode material [18], or the formation of irreversible by-products during the operation of the system [19]. Moreover, since lithium-ion presents not only a higher energy density than zinc-ion battery systems [8] but also a strong control of the mobility market, the later might not be fit for vehicle applications. However, as a result of the large availability of cheap production materials and the high energy density associated with these technologies [8], zinc-ion batteries could become important systems in large scale electric grid and stationary storage solutions in, for example, residential, commercial, and industrial applications.

For the reasons aforementioned above, several companies worldwide have invested in the development of zinc-ion battery cells. Such is the case of Enerpoly AB in Sweden, the company where this thesis was performed. Enerpoly AB was founded in 2018, and since then has researched and continuously developed to commercialize the zinc-ion cell. The company aims for a non-hazardous fully recyclable battery cell, which accounts for 80% less carbon impact and 35% cost savings compared to the average battery product currently in the market [20].

One of the most important steps when developing the manufacturing and assembling processes of a battery cell is establishing a grading and quality control system. The grading of a battery cell is based on the evaluation of its internal (as capacity, voltage, internal resistance, among others) and external (including shape, weight, case sealing) characteristics, and is essential to be performed before its integration in a battery pack [21]. This process, complemented with quality control checks, is not only necessary to discard malfunctioning cells, which should then be either disposed or recycled according to industry standards, but also to divide and sort out the higher from the lower performing functioning cells. In order to increase the performance of a battery pack, consistency is essential, and so these should be constituted of graded cells with similar internal and external properties [22].

For this purpose, after finishing developing their cells, companies must run several tests in a large number of distinct cells, to understand the spectrum of what constitutes a high-quality to a low-quality system. Analysing the results of these tests is essential to comprehend how to divide and sort the produced cells, so that a high-quality consistent product always reaches the customer.

In that regard, the main aim of this thesis is to establish a grading and quality control methodology implementable in the manufacturing, assembly and formation of the battery cells developed by Enerpoly AB. For this purpose, several distinct tests were run in zinc-ion pouch cells, assembled using the electrodes and electrolyte manufactured by the company.

Since zinc-ion batteries are a recent, still under study, technology, no literature on the grading and quality control of these systems is currently available. For this reason, a study was performed to understand if the methods used in the more mature lithium-ion industry could be applied to the zinc-ion chemistry. Moreover, since Enerpoly AB will only assemble and form the cells at the factory, comprehending how these processes influence the behaviour of the final commercial

product is of the most importance. Therefore, with this intent, the scope of the thesis was enlarged to include the analysis of the existence of correlations between parameters associated with the formation and self-discharge of the produced cells and their good or bad functioning defined by the grading method. Finally, by investigating the internal electrochemical mechanisms and variables of the cells while cycling, a relation between the cell's poor behaviour or end-of-life performance and some external factors that could influence its operation was investigated.

To summarize the main objectives of the thesis, a series of research questions were posed:

- Can the grading of zinc-ion battery cells be performed using the same methodology as for lithium-ion cells?
- Which tests should be included and what protocol used in the grading and quality control of the zinc-ion battery cells produced by Enerpoly AB?
- Is there any relation between the formation cycle and self-discharge parameters and the good or bad performance of the battery cells?
- How do external factors related to manufacturing and assembly influence the performance of the battery cells?

In order to explain the methodology and results obtained during the thesis internship and used to assess and reach conclusions to all these research questions, the report is divided into 9 sections. While on this section the motivation, background and goals of the thesis were discussed, in section 2, the state-of-the-art review is presented. As such, section 2 is divided into 3 subsections focusing first on the zinc-ion battery system in general, then in the specifications of the components that composed the used battery cells, and lastly on the grading and quality control tests performed currently in the industry. A detailed description of the method used for the assembly of the pouch cells is then provided in section 3. Afterwards, section 4 presents the results and conclusions from the primary tests that were performed as a way of evaluating a possible protocol and methodology. In this section, an unexpected self-discharge curve shape was observed, and its causes are investigated in section 5. Having understood what problem was influencing the self-discharge curves, more of these tests were completed and their results explained in section 6. Subsequently, in section 7, an extensive analysis on the results achieved from the cycle life tests is explained, with conclusions being drawn in the end. Finally, sections 8 and 9 contain the final conclusions of the thesis and the proposed future research, respectively.

2 State-of-the-art Review

2.1 Zinc-Ion Battery System

Due to the high abundance and safety of zinc (Zn) and manganese dioxide (MnO_2), combined with the high ionic conductivity properties of a non-flammable aqueous electrolyte, rechargeable Zn/MnO_2 batteries are considered as one of the best alternatives to replace Li-ion systems [19]. In this battery, zinc is used as the anode, undergoing dissolution to Zn^{2+} during discharging and electrodeposition back to Zn during charging [23]:

$$Zn \leftrightarrow Zn^{2+} + 2e^{-}$$ [E_o = -0.763 V vs SHE (Standard Hydrogen Electrode) [17]] [Equation 1]

Several studies are still in progress to address some issues related to this material such as dendrite formation (which is mainly due to the process of uneven stripping/electroplating in the anode [24]), shape abnormality, and hydrogen evolution reaction [9]. These, added to structural instabilities related to both current density and the system's pH [25], could not only cause short circuits but also the precipitation of zinc oxide (ZnO) [26], which leads to the insulation of the anode surface. The aforementioned issues could restrict the reversibility of the Zn stripping/deposition reaction and therefore impede the coulombic efficiency. Currently, in the industry, the addition of additives is one of the most popular strategies to mitigate zinc dendrite formation and adverse parallel reactions [9].

On the cathode side, manganese-based materials are promising, not only presenting low cost, low toxicity, and high abundancy, but also good chemical properties including high storage capacity [9]. Different MnO_2 polymorphs (α, β, γ, δ, λ), which possess several comparable electrochemical behaviours [11], are used in the literature. Building the desired structural properties of MnO_2 polymorphs with adequate ionic pathways and surface properties could facilitate the transportation and/or accommodation of Zn ions [27], [28]. Furthermore, by connecting the vertices and edges of MnO_6 octahedra unit cells, chain-type, tunnel-type, and layered-type structures can be therefore constructed [9].

Regarding the electrolyte, zinc metal presents good stability in alkaline, neutral, or weakly acidic aqueous electrolytes [8]. In this thesis, the focus will be on weakly acidic aqueous electrolyte based on zinc sulfate ($ZnSO_4$). Excellent battery performances with $ZnSO_4$ electrolyte and MnO_2 cathode have been reported in literature [26], obtaining not only better cycle stability and specific capacity than other electrolyte solutions [29] but also good coulombic efficiency [12].

However, even though some good testing results have been achieved, the underlaying electrochemical reaction mechanism in the cathode still remains elusive [17]. Several mechanism reactions have been proposed to describe the electrochemical behaviour of the manganese oxides (MnO_x) and the structural evolution of polymorphs in the electrode, but among them, three are more consensually believed to explain the reduction-oxidation processes of MnO_2 in $ZnSO_4$ electrolyte [26]:

1. Zn^{2+} insertion and extraction [19];
2. Conversion reaction through H^+ insertion and extraction [23];
3. MnO_2 dissolution and deposition.

In the first process, due to the high charge density of Zn^{2+}, the Zn ion strongly interacts with the MnO_6 octahedra through intercalation and deintercalation phenomena via the tunnels of MnO_x [11]. Moreover, this process is accompanied with the host-structure deformation, leading to manganese ion dissolution (process 3) caused by Mn reduction and disproportionation reactions (which will be mentioned below) [17].

This MnO_2 conversion mechanism is usually accompanied by several parasitic reactions such as:

1. The formation of a layered hydroxide phase at the interface between the cathode and electrolyte. For example, in $ZnSO_4$ electrolyte solution, zinc hydroxide sulfate, $Zn_4(OH)_6(SO_4)$ [ZHS], is commonly formed [30].
2. The formation of manganese oxide hydroxide (MnOOH) [11]:

$$MnO_2 + H^+ + e^- \leftrightarrow MnOOH \text{ [E}_o = 0.73 - 0.839 \text{ V vs SCE [31]]} \qquad \text{[Equation 2]}$$

3. The formation of zinc-manganese spinel ($ZnMn_2O_4$) [32]:

$$2MnO_2 + Zn^{2+} + 2e^- \leftrightarrow ZnMn_2O_4 \text{ [E}_o = 1.5415 \text{ V vs SHE [33]]} \qquad \text{[Equation 3]}$$

Although, currently, researchers agree that there is proton (H^+) involvement in the electrochemical mechanisms of a rechargeable zinc-ion battery (process 2), more details are needed to fully understand its contribution to the charge and discharge process. Moreover, H^+ contribution in processes as the formation of ZHS or MnOOH mentioned above still requires further analysis [17].

The already mentioned intercalation of Zn^{2+} into MnO_2 and following processes drive the formation of Mn^{3+} compounds, which are extremely unstable in acidic or neutral media (due to its high spin electronic configuration of d-orbital, [Mn^{3+}]: [Ar] $3d^4$) [34]. Therefore, this triggers a Mn^{3+} disproportionation reaction, which will lead to this species degrading to form Mn^{2+} ([Ar] $3d^5$) and Mn^{4+} ([Ar] $3d^3$) [26]:

$$2\,Mn^{3+}(s) \leftrightarrow Mn^{2+}\,(aq) + Mn^{4+}\,(s) \qquad \text{[Equation 4]}$$

As a consequence, these ions will react with the zinc and manganese species forming electrochemical inactive species, such as spinal $ZnMn_2O_4$ and/or Mn_3O_4, which will correlate in a loss of reversibility of the MnO_2 dissolution and deposition process [35]. This will worsen the reversibility of the whole electrochemical process occurring inside the battery, diminishing its cycle life, and thus decreasing its performance.

Several studies have shown that the addition of Mn^{2+} to the electrolyte can suppress MnO_2 dissolution [26], improving cyclability and specific capacity of the system [11], by also reducing the formation of $ZnMn_2O_4$ [36]. This common practice of pre-inclusion of Mn^{2+} to the electrolyte can be better explained by looking at the dissolution reaction of MnO_2:

$$MnO_2 + 2H_2O + 2e^- \leftrightarrow Mn^{2+} + 4\,OH^-$$ [E_o = 1,224 V vs SHE [33]] [Equation 5]

As can be seen, by adding Mn^{2+} to the solution, the equilibrium of the equation above is thermodynamically shifted to the left, thus reversing the dissolution reaction of MnO_2. Furthermore, this shift also reduces Mn vacancies for the insertion of Zn^{2+}, which results in lower capacity loss over cycling since less instabilities of the crystal structure are created due to zinc-ion insertion [26].

Lastly, it has been reported that this addition of the manganese-ion could decrease the formation of zinc hydroxide sulfate [26]. Even though ZHS could prevent the formation of $ZnMn_2O_4$ by buffering the pH of the system [37], the reduction of this ZHS compound presents the advantage of less precipitate blocking the active area of the electrode, which facilitates the interface ion diffusion, therefore enhancing battery rechargeability [26].

Concisely, the three main cathodic reactions affecting the mechanism of the battery are shown below [26]:

$$MnO_2 + 2H_2O + 2e^- \leftrightarrow Mn^{2+} + 4OH^-$$ [E_o = 1,224 V vs SHE [33]] [Equation 6]

$$Zn_{1-x}MnO_2 \cdot nH_2O + xZn^{2+} + 2xe^- \leftrightarrow ZnMnO_2 \cdot nH_2O$$ [Equation 7]

$$4Zn^{2+} + SO_4^{2-} + 6OH^- + 5H_2O \leftrightarrow Zn_4SO_4(OH)_6 \cdot 5H_2O$$ [Equation 8]

Above, the discharging reactions are the ones that occur from left to right, and the charging ones from right to left.

The first one, already mentioned previously, describes the dissolution of MnO_2 in the solution. On the other hand, the second equation describes the insertion (or extraction) of Zn^{2+} in the crystal structure of MnO_2 (x denoting the number of reversibly inserted zinc-ions). As mentioned above, some studies have also concluded that the electrodeposited MnO_2 can also experience proton (H^+) insertion processes [19]. Lastly, the precipitation (or dissolution) of the zinc hydroxide sulfate (Equation 8) at the MnO_2 electrode-electrolyte interface simultaneously occurs due to the presence of hydroxide ions (OH^-) from the first reaction [26].

Contrarily to the lithium-ion battery chemistry, Zn/MnO_2 batteries present charge-discharge curves that can be roughly divided into 2 regions, separated by an inflection point. A general schematic of these curves is presented below for a better visualization [17]:

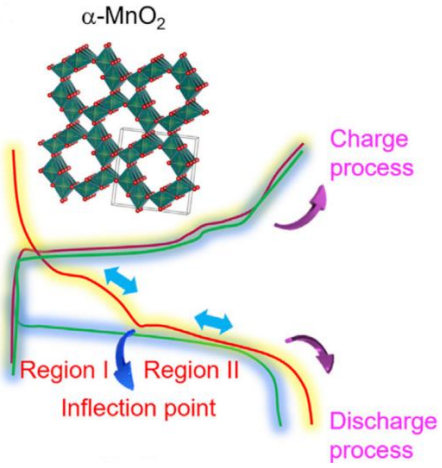

Figure 1– Representative charge-discharge curve of Zn/MnO_2 batteries [17].

During discharge, research has shown that both proton (H^+) and Zn^{2+} insertion (described by Equation 7) magnitudes are much higher in Region I [38], from which it can be concluded that these processes mainly happen in this region, even though they are also present in Region II (being less distinguishable due to the strong chemical conversion reaction of ZHS [17]). On the other hand, both the dissolution of MnO_2 and the formation of zinc hydroxide sulfate control Region II. These intercalation and dissolution reactions, which govern discharge, are affected by the electrolyte pH [17]. The presence of Mn^{2+} additives will delay MnO_2 dissolution (Equation 6), and therefore the formation of OH^- necessary to reach a sufficiently high pH for the zinc hydroxide sulfate formation reaction (Equation 8). In summary, while at relatively low pH the processes happening in the system are mainly the intercalation of zin-ion and the dissolution of manganese dioxide, when a sufficient quantity of OH^- is reached ZHS nucleation begins. Regarding the discharge curve, this nucleation process of the sulfate marks the inflection point, continuing throughout Region II. The pH in Region II is then kept approximately constant since the formation and accumulation of ZHS buffers the generation of hydroxide ions [17]. Thus, the addition of Mn^{2+} ions to the electrolyte not only affects the pH of the system but also the formation of ZHS, which are important aspects for the behaviour of a Zn/MnO_2 battery system.

Contrarily, during charging, the ZHS opposite reaction, which combined with the presence of Mn^{2+} ions will lead to MnO_2 deposition, and the Zn^{2+} deintercalation will be the processes governing the first and second region of the charge curve, respectively.

2.2 Battery Cell Specifications

The development of rechargeable Zn/MnO_2 batteries is still at its early stage. Since the cell processes and properties are still being studied and developed, the research performed in this thesis will be focused on cell testing, using specifically pouch cells.

For the assembly of the cells, a two-electrode setup without a reference electrode is used, where the two electrodes are separated by a piece of polyethylene (PE) membrane with a thickness of 200 μm.

Regarding the anode, zinc foil is directly used as the electrode in the cells.

The preparation of the MnO_2 cathode, on the other hand, involves several steps. First, the mixing of 92 wt.% of manganese dioxide (EMD) powder, 4 wt.% carbon black, 3 wt.% binder, and 1 wt.% suspension agent is performed by a blader to form the slurry. The slurry is then coated on graphite paper or metal foils and passes through an oven to dry. Afterwards, in order to obtain homogeneity, the coated electrode material is taken to the calendaring machine to be calendared. The thickness used for the cathode is controlled at approximately 100 μm. Finally, the electrodes are cut into the right dimensions.

Lastly, the basis of the electrolyte is a 2 M $ZnSO_4$ (zinc sulfate) solution with an added 0.1 M $MnSO_4$ (manganese sulfate) solution. As mentioned in the previous section, the solution of $MnSO_4$ has the intent of adding Mn^{2+} to oppose the dissolution of manganese dioxide, improving the rechargeability and performance of the system [26]. Additives are also added to the mixture to improve homogeneous deposition in the anode and to reduce the overall surface tension in the contact layer between the electrolyte and electrodes. Overall, this results in an electrolyte with a pH of slightly below 5.

The specific process for the assembly of the pouch cells is described in section 3.

2.3 Battery Grading

2.3.1 The Importance of Battery Grading

The battery system manufacturing process can be divided into 2 parts: cell manufacturing and module/pack manufacturing. Between the two processes, when the cell is complete, it is necessary to perform the characterization of its performance [39]. This process is designated by battery grading. Commonly, battery cells are divided into 4 grades [21]:

- Grade A Cells – Represent the best quality cells and have passed all standard quality tests;
- Grade A- Cells – Constitute grade A cells that have been stocked for a longer time;
- Grade B Cells – Lower quality cells that do not meet all criteria establish from the standard quality tests;
- Grade C Cells – Cells that are considered not working properly and should be either destroyed or recycled by following industry standards.

After the grading process, the battery cells are sorted out according to the attributed grade and will eventually be combined into modules or packs. It is essential that these are assembled using similar graded individual cells not only to ensure the whole battery pack is being charged and discharged at the same rate (reliable cell

balancing) and its lifetime and cycle life extended as much as possible, but also to guarantee battery safety for the consumer [40].

Several parameters will influence the grading system of battery cells, but, according to a customer requirement analysis performed [41], these quality features can be divided into 4 categories:

1. Geometry
2. Safety
3. Lifetime
4. Performance

Even though the geometric characteristics of the cell, which include its dimensions and weight [42], might not directly influence its performance, they can directly affect their usability for certain applications and therefore should be included as a quality parameter. Moreover, the already mentioned safety features of the cell outline both its reliability, specifying the general risk level expected in case of cell malfunctioning (which is characterized by data collected from safety and abuse testing [43]), and stability (specially of its active materials) [41].

More important are the lifetime and performance quality features since these directly impact the operation of the cell, and therefore of the whole battery system. While the lifetime features are related to the cyclic stability, calendric and cycle life of the cell, the performance characteristics are quantified by critical performance values such as: achievable capacity, operating voltage, internal-resistance, self-discharge, and capacity recovery [41], [42].

As mentioned before, all these parameters, which will be used to attribute a specific grade to the cells, have to be compared to standard values for each cell manufactured. Therefore, while developing a new battery system technology, establishing a quality and consistency control through a grading system is of the most importance. Only by creating this standard, a company can guarantee that a high-quality consistent product always reaches the customer.

For this purpose – of reaching this quality standard that the following produced cells must comply – after finishing cell development, a company must proceed to run several tests on a considerable number of cells to understand the spectrum from what constitutes a high-quality cell (which will then be attributed grade A) to a low-quality one (grade C). This primary testing must not only evaluate the initial characteristics of the manufactured cells (as the capacity, voltage, and internal resistance) but also study the cell behaviour until its post-mortem status (to reach the final values for calendric and cycle life). Hence, if the standards are defined based on a high number of tests, strong correlations can then be reached between the previously so called initial and final characteristics, enabling to predict the latter based on the former. Therefore, ideally, after establishing the grading system, only the post-formation testing needs to be performed, since everything can be concluded from those, and thus the cells graded and sorted.

To summarize, establishing a grading and quality control system allows the companies to guarantee a high-quality consistent product to the customer, by

evaluating and sorting their manufactured cells through only some simple testing on the fresh and formed cells.

2.3.2 Tests performed for Battery Grading

Since zinc-ion rechargeable batteries are still under development, no literature exists on battery grading and quality control testing for this chemistry. For this reason and the purpose of this thesis, the tests currently used for establishing the grading standards for the more mature lithium-ion battery chemistry will be adopted and applied on zinc-ion cells. This will be the first step to understand if the same processes can still be transferable to this chemistry, and further modification of these grading steps will be evaluated based on the outcome.

Currently, 3 already mentioned parameters are used to define the performance (and therefore the grade) of lithium-ion cells: cell capacity, internal resistance, and open circuit voltage (OCV) [22]. While cell capacity tests aim to define the maximum capacity under a given load, OCV and resistance tests give information on the cell thermodynamic properties and cell dynamics, respectively. These can be used to quantify cell degradation since presently the scientific community agrees on assessing cell aging through capacity fade (capacity loss) and power fade (internal resistance increasing) [44]. Nevertheless, to reach the previously mentioned necessary correlations to define the grading system, self-discharge tests and cycle life tests also need to be conducted.

2.3.3 Capacity Test

The quantity of electric charge which can be accumulated during the cell's charge process, stored during an open circuit period, and then released during the discharge in a reversible way, corresponds to the battery capacity [45].

The conventional method to measure the achievable capacity of the cell is to first fully charge and then discharge it with a low current density. During the latter step, Coulomb counting method is used for the time integration of the current [44]. In this method, the discharged current is integrated from a completely charged stated (at t_0) until a certain voltage threshold, usually designated cut-off voltage ($U_{cut\text{-}off}$), is reached (at $t_{cut\text{-}off}$). Therefore, the capacity of a battery cell can be expressed as [45]:

$$C = \int_{t_0}^{t_{cut-off}} I \, dt \qquad \text{[Equation 9]}$$

Hence, when the cell is discharged with a constant current, its capacity can be easily calculated with:

$$C = I \times \Delta t_{Discharge} \qquad \text{[Equation 10]}$$

Where $\Delta t_{Discharge}$ is the discharge duration. Typically, this time interval is expressed in hours, and thus the usual unit for battery capacity is ampere-hour (Ah).

An important battery parameter related to the capacity is the C-rate. This governs the charging and discharging rates of the whole system [46]. A fully charged battery with 1 Ah capacity rated at 1 C means that it should provide a current of 1 ampere (A) for 1 hour. Additionally, the same battery discharged at a C-rate of 0.5 C provides 500 mA for 2 hours, and at 2 C delivers 2 A for 30 minutes. Therefore, a C-rate of 1 C can also be thought of as that the cell will be fully discharged after 1 hour discharge, while 0.5 C or 0.2 C means the cell will be fully discharged for 2 hours or 5 hours, respectively, and so on.

Regarding the testing protocol for evaluating the achievable capacity, the charging step is usually performed via a constant-current profile followed by a constant-voltage profile with a low current cut-off. For this, not only the intended voltage of the cell has to be defined but also the charging time for the constant-voltage part. On the other hand, the discharge is frequently performed with a constant current [47]. For this step, the desired end-voltage (cut-off voltage) has to be set.

Although this test presents several advantages, as being easily repeatable and barely subjected to current measurement errors [44], some conditions must be guaranteed for reliable results since the capacity of a cell highly depends on both current rate and temperature [48]. Below, a graph showing the correlation between the capacity of a lithium-ion battery system and the temperature is presented.

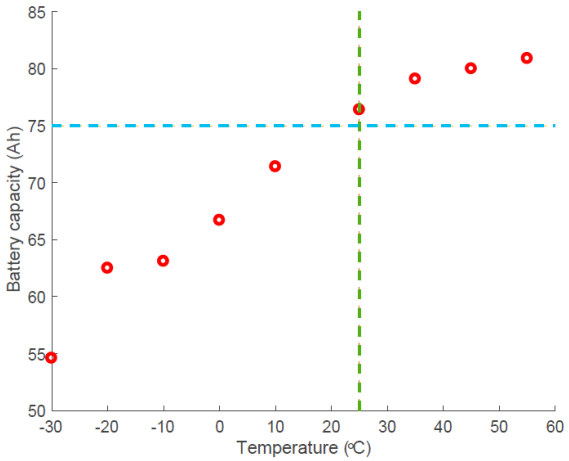

Figure 2 – Correlation between capacity and temperature for a lithium-ion battery [49].

Therefore, in order to obtain consistent results, the tests should be performed in a temperature-controlled chamber.

2.3.4 Open Circuit Voltage (OCV) Test

The open circuit voltage (OCV) expresses the voltage difference between the two terminals of the cell when no current flows through the system (none is either drawn or supplied) [50]. This system condition implies that the terminals are not externally connected, which corresponds to an infinite equivalent resistance ($R_{eq} = \infty$).

The relation between OCV and the state-of-charge (SoC) of a battery needs to be known, so OCV tests measure this equilibrium voltage of the cell as a function of SoC, from 0% to 100% [51]. Therefore, it is not only important that the cell is discharged in known SoC steps but also that it reaches its equilibrium status before the OCV measurement. For this reason, establishing the OCV curve for a certain battery chemistry can require a long time. Furthermore, since the relation between this parameter and SoC also depends on whether the measurements are performed during charging or discharging, this also complicates the evaluation [52]. A possible experimental procedure to obtain the desired relation between OCV and SoC is presented below:

Table 1– Experimental procedure for the measurement of OCV as a function of SoC [51].

Step	Experimental Procedure
1	Constant Current Charge
2	Constant Voltage Charge
3	Voltage Relaxation with Time Limit and Measurement
4	Partial Constant Current Discharge with Capacity Limit
5	Voltage Relaxation with Time Limit and Measurement
6	Repeat Steps 4 and 5 until U_{limit} is reached
7	Partial Constant Current Charge with Capacity Limit
8	Voltage Relaxation with Time Limit and Measurement
9	Repeat Steps 7 and 8 until U_{limit} is reached

As can be seen, the protocol starts by charging the cell to its maximum capacity (by performing a constant current (step 1) and constant voltage (step 2) charging, as explained in the previous section), followed by a resting step to guarantee the cell is in equilibrium for the OCV measurement at 100% SoC. Steps 4, 5 and 6 describe the OCV measurements for the discharging process of the cell, also assuring that the cell reaches equilibrium before the next step. Lastly, steps 7, 8 and 9 express the same OCV measurements but for the charging process.

The resulting curve from these measurements is defined by the OCV curves of both the positive and negative electrodes [44]. These electrode potentials are a consequence of thermodynamic phenomena as the number and types of phase transitions undergone by the materials when the cell is charged or discharged, and the amount of ion intercalated in each phase [53]. Moreover, since, as mentioned above, the pH of a zinc-ion battery system varies with its state-of-charge, the electrode potentials will also depend on this parameter.

As in capacity, these tests should be performed in controlled environments since the relation between OCV and SoC is temperature dependent [54], as can be seen from the graph below:

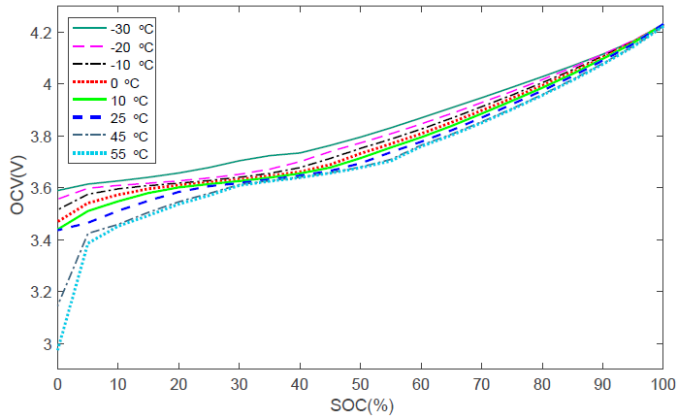

Figure 3 – SOC-OCV relation at different temperatures for a lithium-ion battery [49].

2.3.5 Internal Resistance – Pulse Power Test

Currently, two different methods are mainly used to determine the internal resistance of a cell: pulse power tests and electrochemical impedance spectroscopy (EIS) test.

Pulse power tests, also known as hybrid pulse power characterisation (HPPC), are a simple and short method of obtaining the cell's internal resistance, involving the measurement of the voltage drop resulting from applying a high square-wave direct current (DC) to the cell [44]. Therefore, the internal resistance (iR) can be calculated from:

$$iR = R_{pulse} = \frac{\Delta V}{\Delta I} = \frac{V_f - V_i}{I_f - I_i} \quad \text{[Equation 11]}$$

Being V_i, V_f, I_i and I_f the initial and final voltage and initial and final current, respectively [22]. This internal resistance of the cell results from a combination of multiple dynamics, that can be divided into 3 different resistances: the ohmic resistance (R_o), the charge transfer resistance (R_{CT}) and the polarisation resistance (R_P). While the first includes all electronic resistances within the cell [55], the second is related to the charge transfer mechanisms at the electrode/electrolyte interface [56], and the third comprises the ionic diffusion in the solid phase [57]. The influence of these 3 resistances (R_o, R_{CT}, and R_P) on the internal resistance is strongly associated with the cell design and assembly [44].

Below, a scheme illustrating the voltage response (ΔV) to a general square-wave discharge current load is shown.

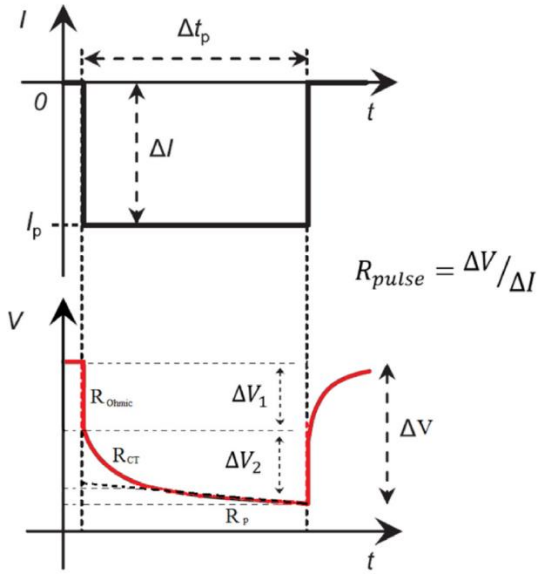

Figure 4 – Schematic of the voltage response to a square-wave current for a pulse power test [44].

As can be seen, the ohmic resistance (R_o) is responsible for the initial voltage drop following the current pulse, the charge transfer resistance (R_{CT}) occurs after a small-time interval of applying the current, and, lastly, the polarisation resistance (R_P) is accountable for the last small voltage reduction.

Lastly, it is important to mention that, as for the open circuit voltage, the internal resistance of a battery cell depends not only on the temperature, as shown by the graph below, but also on the state-of-charge of the cell. Therefore, for consistent results, these tests should also be performed in a temperature-controlled environment.

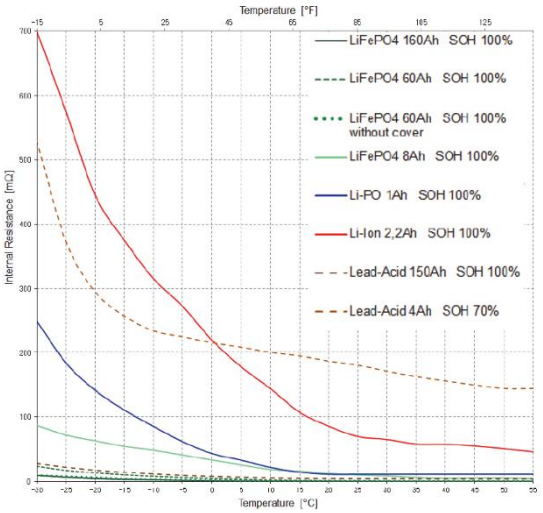

Figure 5 – Internal resistance as a function of temperature for several different chemistries [58].

Since a temperature increase leads to a higher electron mobility and thus higher current produced by the cell, the internal resistance, which opposes ion flow, will decrease with temperature [59], as can be seen by the graph above.

2.3.6 Internal Resistance – Electrochemical Impedance Spectroscopy (EIS) Test

As mentioned above, the second method commonly used to determine the internal resistance of a cell is electrochemical impedance spectroscopy tests. Electrochemical impedance measurements are usually done by applying a sinusoidal (AC) potential to the cell and measuring its current response [44]. As a result, the impedance ($Z(w)$) is obtained as a function of the frequency (w), with the lower and upper frequency limits being defined by the testing time and inductive behaviour of the cell, respectively.

Since the impedance can be divided into its real ($Re(Z(w))$) and imaginary parts ($Im(Z(w))$), it is then typically represented by a Nyquist plot – as the one presented below. These graphs depict the negative imaginary part of $Z(w)$ in the y-axis against its real part on the x-axis.

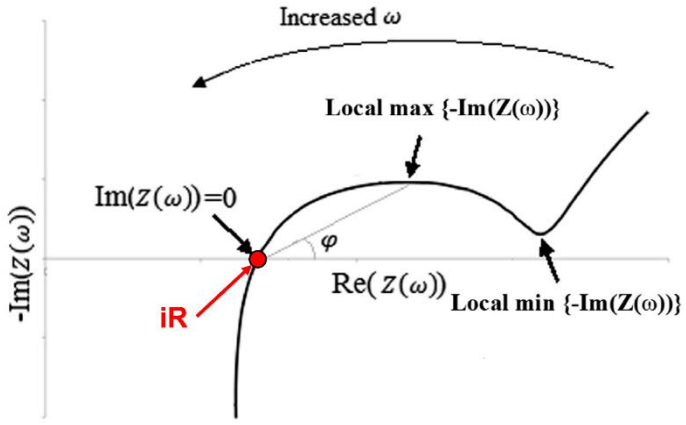

Figure 6 – General Nyquist Plot [44].

Several parameters that affect the cell behaviour can be read from its Nyquist plot. At the point where the imaginary part of the impedance is zero ($Im(Z(w)) = 0$), the cell behaviour changes from capacitive to inductive, and an almost pure ohmic resistance is observed [56], being thus considered as the internal resistance (iR) of the cell. Moreover, the charge transfer resistance (R_{CT}) can also be estimated by calculating the difference between $Re(w)$ at local min $\{-Im(Z(w))\}$ and the internal resistance. Lastly, the 1/RC characteristic frequency of the cell can be read at the point in which $-Im(Z(w))$ presents a maximum. Higher the value of this frequency, faster the voltage of the system changes with fast current [56].

As explained in the last section, since the internal resistance is dependent on the temperature, in order to ensure consistency, these tests must also be performed in a temperature-controlled chamber.

To conclude, since a battery cell is a complex electrochemical cell, presenting non-linear properties and behaviour (as non-linear Butler-Volmer kinetics), it is worth mentioning that the values obtained for R_o and R_{CT} from both EIS and pulse power tests might differ [60].

2.3.7 Self-Discharge Test

The processes that result in a decrease of the performance of electrochemical power sources, as electrochemical cells, without a flow of current through an external system are designated by self-discharge processes [61]. Since these phenomena reduce the shelf life of a battery system, requiring regular monitoring of the system, technologies which present higher self-discharge processes are generally disfavoured by the industry.

Self-discharge tests are usually performed at a specific environmental condition for a fixed period of time. The performance of the battery, which is kept under a load-free system during the entire test, is evaluated by measuring its voltage and capacity reduction [61]. The open circuit voltage measurements are therefore consistently performed after a determined time interval (Δt) in order to obtain a OCV as a function of time curve. Higher the Δt, higher will be the difference between consecutive voltage measurements, and therefore higher the decrease in the state-of-charge of the cell.

An important phenomenon that can affect the interpretation of the self-discharge curve of an electrochemical system is cell relaxation [62]. Cell relaxation occurs both in charging and discharging. When charging, an external voltage is applied to the cell forcing current into its terminals and increasing its voltage and therefore its SoC. After removing this external voltage, the cell internal electrochemical mechanisms will tend to an equilibrium and consequently its OCV will drop slightly. The opposite happens when discharging, where current is drawn from the cell, decreasing its OCV and SoC. After discharge, the OCV will slightly rise as the cell relaxes [63]. Therefore, when performing a self-discharge test, a sufficient amount of waiting time should be given to ensure the cell is done relaxing before the first OCV measurement is performed [62]. Otherwise, this OCV measurement will be the sum of the cell's relaxation and self-discharge effects. Since it is challenging to access the length of the relaxation period, to guarantee consistent results the same relaxation time should be assumed for every cell.

Self-discharge processes are also highly dependent on temperature – higher the temperature, higher the self-discharge rate [64]. For this reason, these tests should be conducted in a temperature-controlled environment. Below, a graph illustrating the self-discharge curve of a lithium-ion cell for different temperatures is presented.

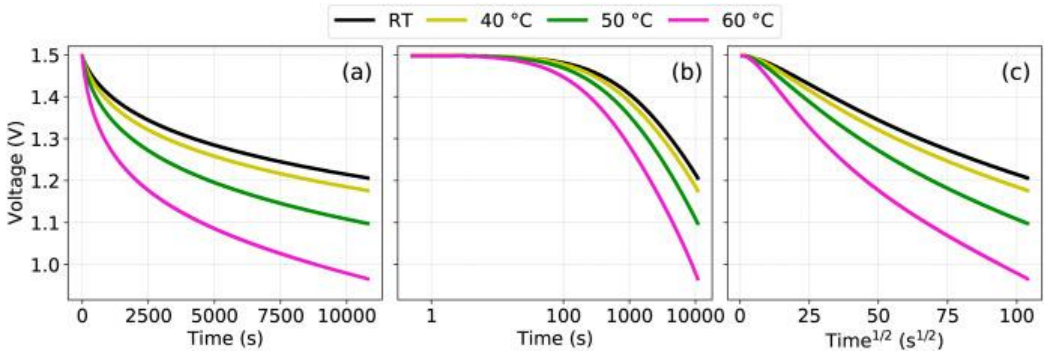

Figure 7 – Self-discharge curves for a lithium-ion cell for different temperatures (a), in logarithmic scale (b) and as a function of time$^{1/2}$ (c) [65].

Moreover, at different SoC of the cell, different self-discharge rates are observed [66], having a higher value for higher SoC.

In the lithium-ion battery industry, one of the 2 following protocols are usually used to access the self-discharge phenomena of these technologies [42]:

- Stock the systems for 28 days at room temperature condition of 25^{0}C (considered more reliable by the industry);
- Stock the systems for 7 days at higher temperature of 45^{0}C.

The second can be explained with the dependence of the self-discharge in the temperature seen in the graphs above. Since higher temperature will lead to a higher self-discharge rate, some companies prefer to test their battery cells in high-temperature conditions in order to reduce the testing time.

Lastly, it is worth mentioning that many companies include self-discharge tests in their quality control protocol for the produced cells as a procedure to exclude faulty and bad-functioning cells. Battery cells that present high self-discharge rates should not be commercialized and instead be recycled according to industry standards. In order to identify these flawed cells, they are fully charged and left to self-discharge for a determined time period. If, by the end of these period, their voltage drop is higher than a pre-determined value (fixed by the grading of the battery cell), they should be disposed or recycled properly.

2.3.8 Cycle Life Test

A battery charge - discharge cycle refers to the process of completely charging and discharging a battery system [67]. The number of charge - discharge cycles that a battery can complete before losing its performance is designated by cycle life [68]. In order to test the cycle life of a battery cell, a series of charge and discharge processes (cycles) are performed until a previously defined standard is reached. Each company (or industry) defines a different standard for what is meant by the loss of performance of a battery system. As an example, lithium-ion battery cells are

normally considered to enter its death status when its achievable capacity is less than 80% of its original capacity [69].

Similarly to the other already mentioned parameters, the cycle life of a battery is also temperature dependent. As can be seen from the graph below, the number of full cycles that the system can complete decreases with temperature. This is mainly due to the fact that at high temperatures, the electrochemical reactions occur at a faster rate, inducing parasitic damaging reactions to the technology.

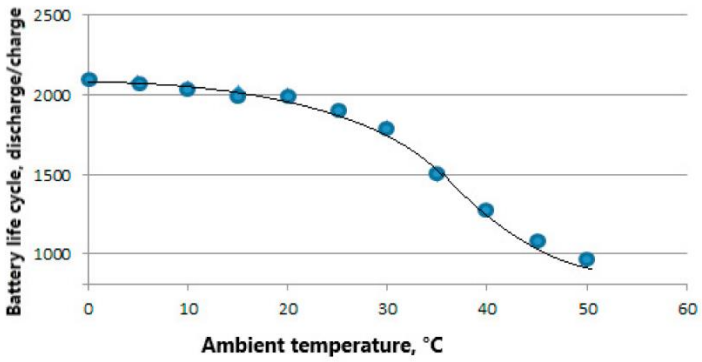

Figure 8 – Influence of temperature on the cycle life of a lithium-ion battery [70].

Moreover, cycle life is also affected by other testing parameters as the C-rate used to charge and discharge the cells. As a result of high C-rates, the active materials of the cells cannot accompany the high current drawn, which leads to incomplete or unwanted chemical and electrochemical reactions, causing capacity fade [71]. Therefore, as can be observed in the graph below, higher the charging and discharging C-rates, faster does the cell achievable capacity decrease and thus lower the cycle life.

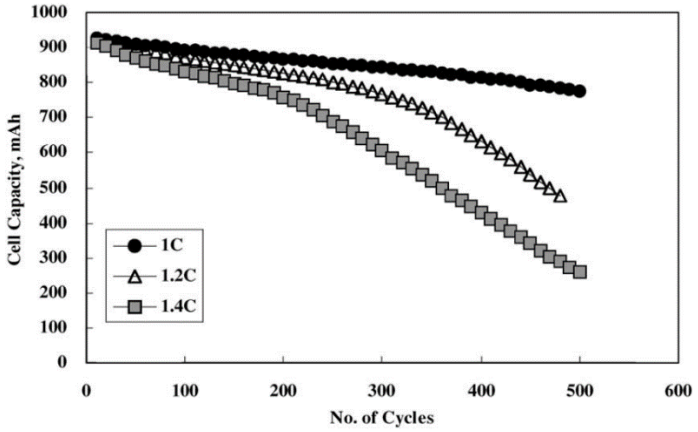

Figure 9 – Effect of C-rate on the cycle life of a LCO lithium-ion battery [72].

The cycle life depends on the total amount of energy charged and discharged that the active materials of the cell can tolerate [71]. Hence, when considering the influence in the battery cycle life, a charge and discharge cycle with 100% depth of discharge (DoD, refers to the amount of charge removed from a battery at a given

state compared to the total amount of charge [73]) is approximately the same as 2 cycles with 50% DoD, 100 cycles with 1 % DoD, and so on. Consequently, in order to greatly increase the cycle life of a battery, the manufacturer can restrict the possible DoD in its application. The high dependence of cycle life on the depth of discharge is illustrated for a zinc-manganese dioxide cell in the graph below.

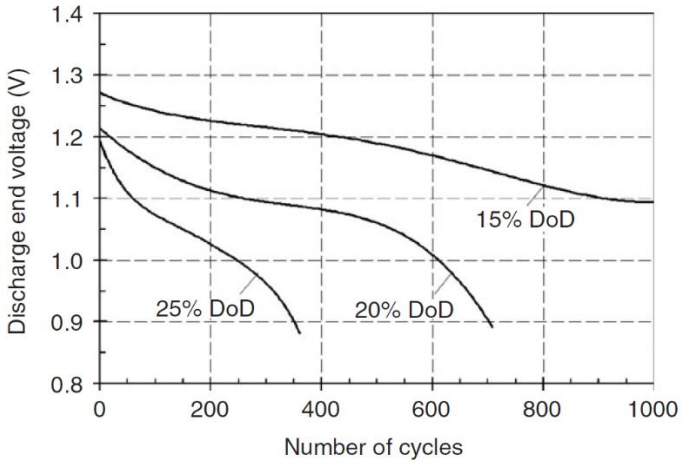

Figure 10 – Cycle performance as a function of the depth of discharge for a rechargeable zinc-manganese dioxide AAA cell [74].

Similarly, by restricting the charging cut-off voltage (the voltage value until which the cell is charged), the cycle life can also be improved [72]. By partially charging the battery cell instead of fully charging it, the total energy associated with each cycle decreases, which results in a lower capacity fade per cycle (analogous to lowering the DoD as explained above). This phenomenon can be observed for different values of charging cut-off voltage in the graph below.

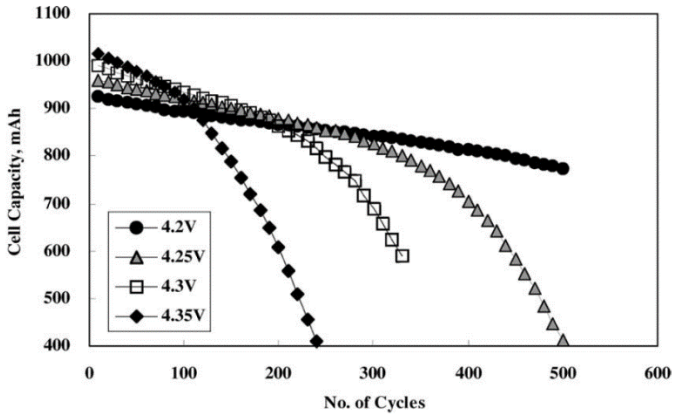

Figure 11 – LCO lithium-ion cell capacity as a function of the number of cycles for different values of charging cut-off voltage [72].

Therefore, in order to achieve consistency in the grading tests, which is essential to reach a reliable quality and control system, all these testing parameters – temperature, C-rate, depth of discharge, and charging cut-off voltage – should be identical between the different tested cells.

2.3.9 Insulation Test

In order to achieve a good performance from the battery system, it is important to guarantee the insulation between not only the anode and the cathode but also the electrodes and the enclosure. For this purpose, the battery cell insulation resistance is measured using an insulation tester, which uses a high-sensitivity ammeter to detect the extremely low current flowing between electrodes when a DC voltage is applied [75]. These tests are usually carried out both before and after filling the electrolyte into the battery cells, to ensure no drawbacks caused by insulation defects or internal shorts. The cells should present a very high internal resistance before the electrolyte filling, which decreases substantially (although still remaining high) after this process.

For this reason, currently in the industry these tests are used mainly as a means to discard defective cells, which due to these defects can become a safety hazard, and therefore should be disposed and recycled.

3 Pouch Cell Assembly

Since the zinc-ion battery chemistry is non-hazardous, emitting no dangerous gases, the assembly of the cells was performed without the use of a glove box. The assembly process of pouch cells can be divided into 5 steps: cathode assembly, anode assembly, pouch bag assembly, electrolyte filling, and cell final sealing.

Regarding the cathode assembly, the process starts by cutting the electrode from a piece containing the coated slurry onto the current collector (graphite paper), which has been previously dried and calendared. The dimension of the electrode is 2 cm by 2 cm. Afterwards, the electrode is weighted in order to obtain its mass loading, by comparing it with the mass of graphite paper with the same dimensions:

$$mass\ loading = m_{electrode} - m_{graphite\ paper} \qquad \text{[Equation 12]}$$

The positive terminal (graphite paper) is then attached to the electrode, in the current collector side, using PEA tape. Moreover, the current collector side is subsequently all covered by the same tape in order to avoid any parasitic reactions, e.g., direct MnO_2 deposition on the current collector (Figure 12 (a) and (b)).

A relatively easier process is used to assemble the anode. The zinc foil is first cleaned using acetone, and then cut into a 2 cm by 2 cm square. Afterwards, the negative terminal (brass) is fixed to one of its sides using the same tape. For this electrode, none of the sides are fully covered by the tape (Figure 12 (c) and (d)).

Having both electrodes assembled, they can be joined with the polyethylene (PE) separator in between. In order to avoid any short circuits or insulation problems, the separator is cut to have slightly higher dimensions compared to the electrodes. The two electrodes are then tapped together with the separator between them (Figure 12 (e) and (f)). The whole is then placed inside a pouch bag with one side left open (Figure 12 (g)). To ensure a complete insulation on the electrodes terminals' side where those terminals need to extend out of the bag, sealant wax paper is applied on the opening area of the bag during heating sealing. Having the bag ready, the electrolyte is filled (from the remaining open side) (Figure 12 (h)). Even though in a first instance the larger air bubbles are taken out manually, the bag is still placed in a vacuum tank at c.a. 100 mbar for approximately 1 hour to guarantee that the leftover air is removed.

After the electrolyte infiltration process, the pouch bag is further closed through heating on its open side with a vacuum sealer, thus creating the final pouch cell (Figure 12 (i) and (j)). After this step, the cell is ready to be connected to the cycler for testing.

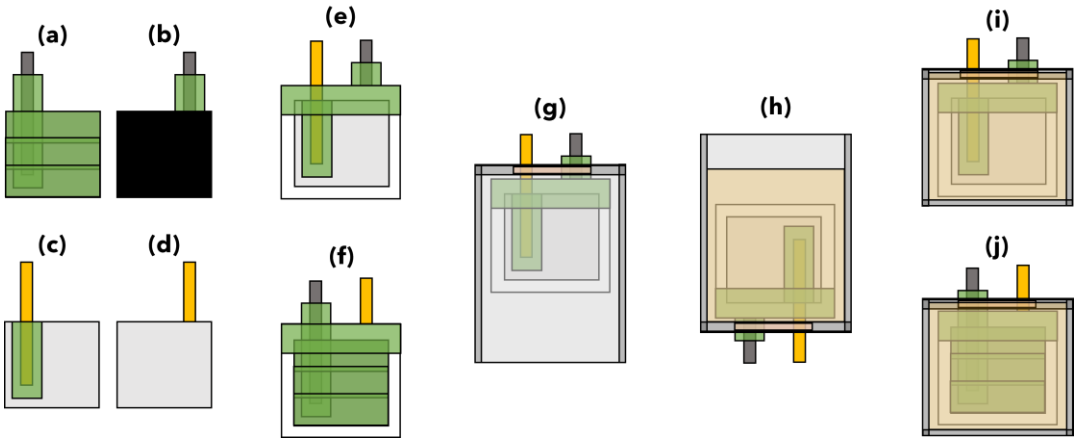

Figure 12– Pouch cell assembly steps: (a) current collector side of the cathode; (b) active side of the cathode; (c) and (d) sides of the anode with and without the negative terminal, respectively; (e) and (f) anode and cathode side, respectively, of both electrodes joint with the separator in the middle; (g) both electrodes and separator in the pouch bag with 3 of its sides sealed; (h) electrolyte filling; (i) and (j) final pouch cell – anode and cathode side, respectively.

Below, pictures taken in the lab of both electrodes, the ensemble before electrolyte filling and the final pouch cell are presented.

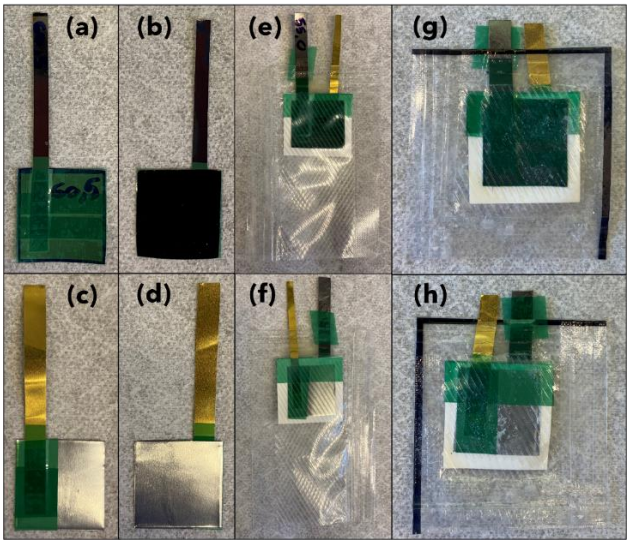

Figure 13 – Pictures taken in the lab of: (a) and (b) current collector and active side of the cathode, respectively; (c) and (d) anode sides with and without the terminal, respectively; (e) and (f) cathode and anode side, respectively, of the ensemble constituted by both electrodes, separator, and cell case; (g) and (h) cathode and anode side, respectively, of the final pouch cell.

4 Primary Cell Testing

4.1 Methodology and Protocol

Initially, in order to assess if the intended testing protocol worked properly for the assembled cells, 2 cells (designated P2231 and P2232) were connected to the NEWARE cycler and analysed. The testing protocol run on the cells were divided into 3 parts: formation cycle part, self-discharge part, and cycle life part – the cells were first formed with one formation cycle, then left to self-discharge for 2 (cell P2231) or 4 weeks (cell P2232), and lastly, for the former cell, continuous charge and discharge cycles were performed to try to determine its cycle life.

The protocol that was used to perform all these tests is presented in Table 2 – where the step time relates to the maximum time each step can take; the voltage limit is the maximum and minimum voltage the cell is brought to when charging or discharging, respectively; the cut-off current is a threshold parameter that terminates the step if the current is too low; and the time record is the time interval between the collection of 2 data points.

As can be seen, the testing protocol starts with an internal resistance measurement using an EIS test (step 1). Afterwards, in order to be formed, the cell undergoes a number of formation cycles (NFC) (step 8), each involving a CC and CV charge to a voltage of 1.75 V (steps 3 and 4) and a CC discharge to a voltage of 1.15 V (step 6). It is worth noticing that, before even starting any step, the cell is rested for 12 hours (step 2) so it can reach an equilibrium state. At the end of every formation cycle, a fast discharge (with triple the current density) is also performed to obtain the DCIR at 0 % SoC (step 7).

After formation, a 2nd EIS is performed (step 9), followed by the self-discharge part of the testing protocol. For this purpose, the cell is charged to 1.75 V (steps 11 and 12) and left to rest for the desired self-discharge time (step 13). In order to obtain the capacity fading rate and internal resistance after self-discharge, a discharge followed by another DCIR test are subsequently carried out (steps 14 and 15).

Lastly, the cells undergo a cycle life test. The cycle life tests are divided into 2 parts – first 2 slow cycles with a low charge and discharge current density (10 mA/g) are performed in order to collect the desired data (including a DCIR discharge in step 21) (steps 17 to 22), and afterwards 20 fast cycles with a much higher charge and discharge current density (60 mA/g) are carried out as a way of quickly ageing the cells (steps 23 to 27). This 2 slow – 20 fast ageing cycle protocol is performed 5 times (step 28) to guarantee that the cell ages sufficiently and enough data is collected. Lastly, in the end, 2 slow current density cycles are again completed to collect the final cycle life data (steps 29 to 34).

The reason for performing 2 slow cycles for data collecting, instead of only one, is the cell's memory effect. The memory effect is the ability of a battery cell to remember its regular usage pattern [76]. For this reason, by recharging the battery before it is completely discharged, operating in a lower window of working voltage (as performed in the cycle life tests), the cell will gradually lose the ability to deliver

its real achievable capacity. Therefore, in order to avoid this effect, 2 slow cycles are performed for data collection, and the values related with the 2nd cycle used.

Lastly, it is worth mentioning that, even though on the table below the current density is presented, the current for each cell is the real input of the cycler program. In order to calculate the specific current for each cell in each step, the following expression is used:

$$I_{cell/step} = mass\ loading_{cell} \times \%EMD \times current\ density_{step} \times Area_{cell}$$

[Equation 13]

Table 2 – Cycler protocol for the different parts of the primary cell testing.

Cycling Part	Step Number	Step Name	Step Time	Voltage Limit [V]	Current Density [mA/g]	Cut-off Current [mA]	Time Record [s]
1st EIS	1	-					
Formation Cycles	2	Rest	12 hr	-	-	-	30 sec
	3	CC Charge	-	1.75	20	-	10 sec
	4	CV Charge	3 hr	1.75	20	0.01	10 sec
	5	Rest	10 min	-	-	-	30 sec
	6	CC Discharge	-	1.15	20	-	10 sec
	7	CC DCIR Discharge	3 sec	-	60	-	0.1 sec
	8	Cycle	Start Step: 3 Cycle Count: NFC				
2nd EIS	9	-					
Self-Discharge Test	10	Rest	10 min	-	-	-	30 sec
	11	CC Charge	-	1.75	20	-	10 sec
	12	CV Charge	3 hr	1.75	20	0.01	10 sec
	13	Rest Self-Discharge	Self-Discharge Time	-	-	-	30 sec
	14	CC Discharge	-	1.15	20	-	10 sec
	15	CC DCIR Discharge	3 sec	-	60	-	0.1 sec

Cycle Life Tests	16	Rest	10 min	-	-	-	30 sec
	17	CC Charge	-	1.75	10	-	10 sec
	18	CV Charge	3 hr	1.75	10	0.01	10 sec
	19	Rest	10 min	-	-	-	30 sec
	20	CC Discharge	-	1.15	10	-	10 sec
	21	CC DCIR Discharge	3 sec	-	60	-	0.1 sec
	22	Cycle	Start Step: 17 Cycle Count: 2				
	23	CC Charge	-	1.75	60	-	10 sec
	24	CV Charge	3 hr	1.75	60	0.01	10 sec
	25	Rest	10 min	-	-	-	30 sec
	26	CC Discharge	-	1.15	60	-	10 sec
	27	Cycle	Start Step: 23 Cycle Count: 20				
	28	Cycle	Start Step: 17 Cycle Count: 5				
	29	CC Charge	-	1.75	10		10 sec
	30	CV Charge	3 hr	1.75	10	0.01	10 sec
	31	Rest	10 min	-	-	-	30 sec
	32	CC Discharge	-	1.15	10	-	10 sec
	33	CC DCIR Discharge	3 sec	-	60	-	0.1 sec
	34	Cycle	Start Step: 29 Cycle Count: 2				
End	35	-					

4.2 Results and Discussion

As mentioned in the previous section, the two cells that were used for the primary testing (cells P2231 and P2232) had different testing protocols. Although both were formed with 1 formation cycle (NFC = 1 in Table 2), cell P2231 underwent a self-discharge rest of 2 weeks followed by cycle life test, while cell P2232 only performed a 4-week self-discharge test with no cycle life test (the reasons will be explained later). Below, the cycling profiles of the cells for their complete respective protocols are presented.

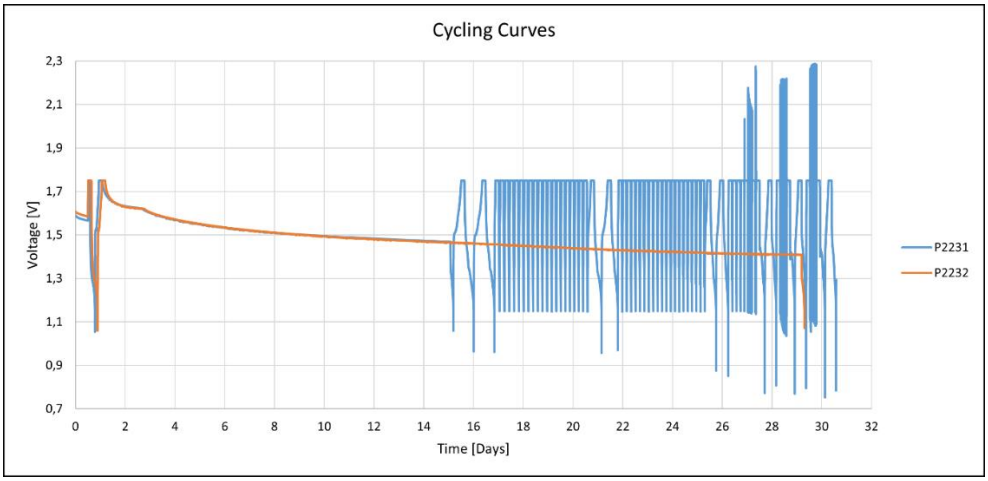

Figure 14 – Cycling Curves for Cells P2231 and P2232.

Even though, according to the already existing literature on zinc-ion chemistry [77], [78], the self-discharge curve of these battery cells should present only one plateau (resembling the curves of the more studied lithium-ion chemistry) it was observed that, for the studied cells, the curves (in more detail in Figure 15 (a)) present 2 plateaus, with a voltage drop between the 1st and 2nd resting day. In order to evaluate and explain this 2-plateau self-discharge curves, 3 hypotheses were proposed and investigated (results and discussion in section 5):

1. The voltage drop that creates the two-plateau curve could occur due to the cell not being fully formed, and hence 1 formation cycle is not sufficient. To check the validity of this hypothesis, 6 cells were assembled and formed with a different number of cycles (2, 3 and 5) to analyse if the self-discharge voltage drop would still appear – results in section 5.1.
2. The voltage drop could also result from a parasitic reaction involving the current collector. These reactions have already been observed in the lithium-ion chemistry [79], but no literature was found for zinc-ion systems. Therefore, to test this hypothesis, 2 cells were assembled with stainless steel current collectors and left to rest for 2 weeks – results in section 5.2.
3. Lastly, as can be seen in Figure 14 and Figure 15 (a), the voltage drop occurs for both cells at the same time. This could suggest that the reason for the 2-plateau curve is not related to chemical or electrochemical processes happening inside the cell but rather due to the equipment used for the

testing. A small current leakage from the cycler's channels could discharge momentarily the cell causing its voltage to drop – conclusions on section 5.3.

Regarding the cycle life test performed on cell P2231, it can be seen in Figure 15 (b) that around the 12th day – approximately cycle 50 – the cell starts to present a strange behaviour. This malfunctioning of the cell could be explained by 2 factors. First, since the pouch cell has been tested for a period longer than 1 month, the electrolyte inside could start to dry out, thus hindering the ion movement in the cell, resulting in a poor performance [80]. However, since these unusual readings only happen for the fast cycles, this malfunctioning could also be associated with the current density used for the fast charge and discharge cycles. By charging and discharging the cell with a high current, the system is subjected to a high flux impact, therefore leading to a high internal resistance feature, which could explain the strange plateau and voltage readings seen in Figure 15 (b). For this reason, in order to avoid these problems in the future cycle life tests, the current density used for the fast charge and discharge cycles was reduced to 40 mA/g. Moreover, since for these cells only 5 slow cycle data points are collected (every 20 fast cycles), which is not enough to understand if a (capacity or internal resistance) trend exists, in future tests the protocol was also altered to have 2 slow cycles every 10 fast cycles, doubling the number of data points.

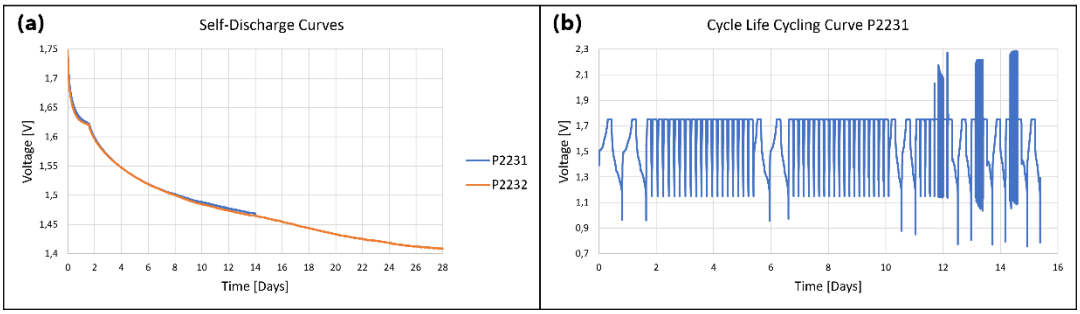

Figure 15 – (a) Self-Discharge curve for cells P2231 and P2232; (b) Cycle life cycling curve for cell P2231.

5 Study of the 2-Plateau Self-Discharge Curve

5.1 Self-Discharge with Different Number of Formation Cycles Testing

5.1.1 Methodology and Protocol

As mentioned above, one of the hypotheses stipulated for the unpredicted 2-plateau self-discharge curve seen in the primary tests was that the studied cells were not fully formed. For this reason, in order to study the influence of the number of formation cycles in the behaviour of the system, 6 cells were assembled and formed with a different number of cycles:

- Cells P2255 and P2256 were subjected to 3 formation cycles (NFC = 3);
- Cells P2257 and P2258 were subjected to 5 formation cycles (NFC = 5);
- Cells P2289 and P2290 were subjected to 2 formation cycles (NFC = 2).

In addition to studying the relation between the number of formation cycles and the self-discharge curve, these tests served another purpose. Since, when creating a grading system, the target is to associate the initially measured parameters with the performance of the cell, it is important to understand what parameters should be evaluated and collected from the formation cycles. Moreover, by studying and understanding the correlations between these parameters, the amount of collected data in future tests could be significantly reduced, facilitating the process from a computational perspective. Therefore, for each cycle, values of several different parameters were collected and analysed, attempting to correlate them. As a way of increasing the number of data points and consolidate the identified relations, the data points related to cells P2231 and P2232 were also employed.

The cycling protocol used on these cells is similar to the one presented in Table 2 without the cycle life part. The cycling curve for the formation cycles part for the 8 cells is presented below:

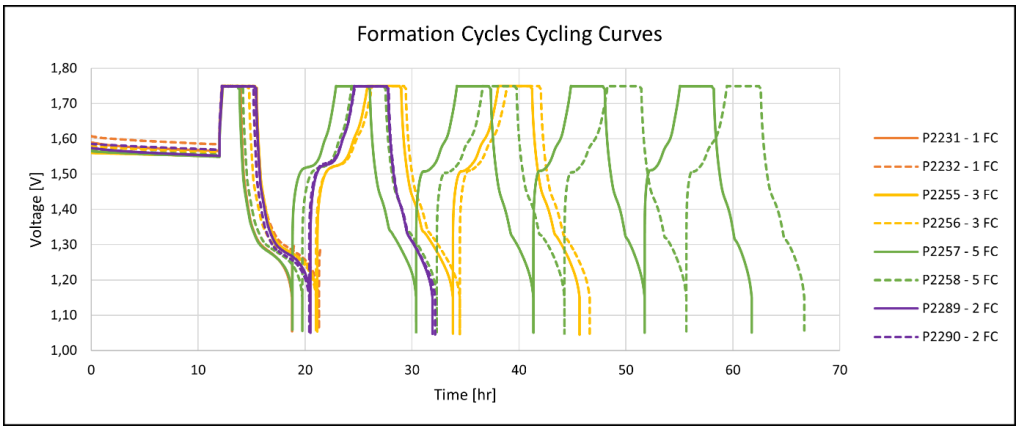

Figure 16 – Formation Cycles Cycling Curves for the 8 tested cells.

5.1.2 Correlations between Formation Cycle Parameters

As mentioned, on a first instance, a study was performed to find correlations between the parameters related to each formation cycle. By doing so, if strong correlations are found, instead of several parameters only few could be used in the analysis, since they would provide the same information. Below, as an example, the charge and discharge curves for each formation cycle of cell P2257 (which was subjected to 5 formation cycles) are presented. It is worth noticing that, for every cell, the discharge profile related to the 1st cycle presents a different shape and behaviour compared to the other cycles (as can be seen in Figure 17).

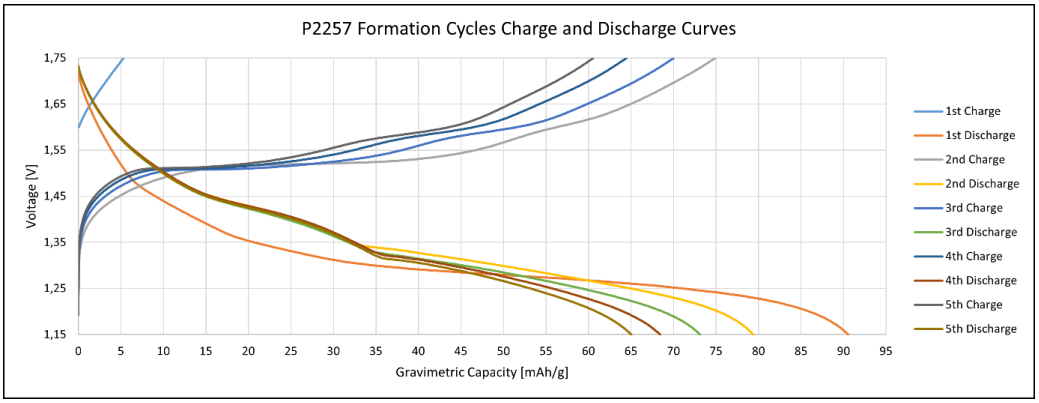

Figure 17 – Charge and discharge curves of cell P2257 for each formation cycle.

With this intent, for each charge and discharge cycle several parameters were measured and collected. Depending on the stage they have been obtained in, the collected parameters can be divided into 3 different categories:

- Initial state parameter – parameters collected prior the formation cycles;
- Cycling state parameter – parameters collected every formation cycle;
- Final state parameter – parameters collected after the formation cycles.

Table 3 presents every formation cycle parameter collected divided into the 3 distinct categories:

Table 3 – Formation cycle parameters divided into 3 categories.

Initial State	Cycling State	Final State
Initial EIS Internal Resistance	Voltage Drop after Charge	Final EIS Internal Resistance
Initial Voltage before Resting	Median Discharge Voltage	-
Final Voltage after Resting	Average Discharge Voltage	-
Resting Voltage Drop	Charge DCIR	-
First CV charging time	Discharge DCIR	-

Mass Loading	Discharge Capacity	-

The initial and final EIS internal resistance refer to the internal resistance values obtained by the EIS tests performed before and after the formation cycles, respectively. On the other hand, as can be seen in the protocol presented in Table 2 and also in the cycling curves shown in Figure 16, before formation, the cell is left to rest for 12 hours. The initial, final, and resting voltage drop are related to this resting period. Moreover, the first CV charging time accounts for the interval of time that the cell takes in step 4 of the protocol. To be noticed that although 3 hours were set for the first CV step, this step could still be terminated due to the extreme low current response (0.01 mA/cm^2), therefore obtaining different charging times between different cells. This can only happen at the first CV step when cells are still fresh. After the formation cycle, each cell can be held at CV step for 3 hours without interruption. Furthermore, for each formation cycle, the voltage drop between the charge and discharge steps was measured, the median and average voltage of the discharge process calculated, and the internal resistance from the charge and discharge DCIR obtained. Lastly, the final discharge capacity of each formation cycle is also evaluated.

Even though all these parameters can be obtained from the data collection before, during and after the formation cycles, not all will be employed to study the desired correlations. On one hand, the initial and final voltage of the 12-hour resting period will not be used in the study, since the voltage drop related to this time interval not only can provide more information but also is an easier parameter to compare between cells. On the other hand, the charge DCIR is dismissed since the program's calculation process occurs for the beginning of the charging process, when the SoC is close to zero, which is at approximately the same cell state as for the calculation of the discharge DCIR and will then present the same information.

Therefore, the study will analyze the correlations between the following parameters:

Table 4 – Formation cycle parameters analysed in the correlation study.

Initial State	**Cycling State**	**Final State**
Initial EIS Internal Resistance	Voltage Drop after Charge	Final EIS Internal Resistance
Resting Voltage Drop	Median Discharge Voltage	-
First CV charging time	Average Discharge Voltage	-
Mass Loading	Discharge DCIR	-
-	Discharge Capacity	-

In order to correlate the parameters, two independent ways to analyze the data were investigated. First, each formation cycle was studied independently, using the values of each cell for only the specific cycle. Second, each individual data point is treated as an independent case, without regard to which cell or cycle it belongs. Therefore,

while in the first approach only the data points from each respective cycle are used to find relations between themselves, in the second all the collected data points are studied as a whole.

For the first formation cycle, the data of all the 8 cells was used to study the parameters. The relations found are presented in the graphs below (Figure 18). First, a linear relation was observed between the voltage drop after the first charging step and the first CV charging time (Figure 18 (a)). Since a shorter charging time could result from a slightly higher internal resistance of the cell, and this parameter affects proportionally the voltage drop, it is understandable that an increase in charging time could translate in a smaller voltage drop between charging and discharging. On the other hand, the discharge DCIR after the first formation cycle and the internal resistance measured by the initial EIS could be linearly related (Figure 18 (b)). However, it is worth noticing that the value of R^2 (the coefficient of determination, which provides statistical information on how well the regression line approximates the real data [81]) is not very high and the data points for lower EIS internal resistance dispersed. Therefore, more data would need to be collected to understand this relation better. Lastly, an unexpected relation was obtained between the internal resistance measured by the final EIS and the voltage drop of the initial 12-hour rest (Figure 18 (b)). Nevertheless, once again the value of R^2 is not very high for the collected data points. In addition, it is not understandable why a parameter that is measured before the formation cycles could be related to a parameter collected after. So, once again, more data should be collected to verify this relation.

Regarding the other parameters, no more relations were found between them for the 1st formation cycle values. A parameter that did not show any clear strong correlations, presenting quite dispersed values between cells and thus seeming either completely independent or non-related to the others, was the internal resistance measured from the initial EIS.

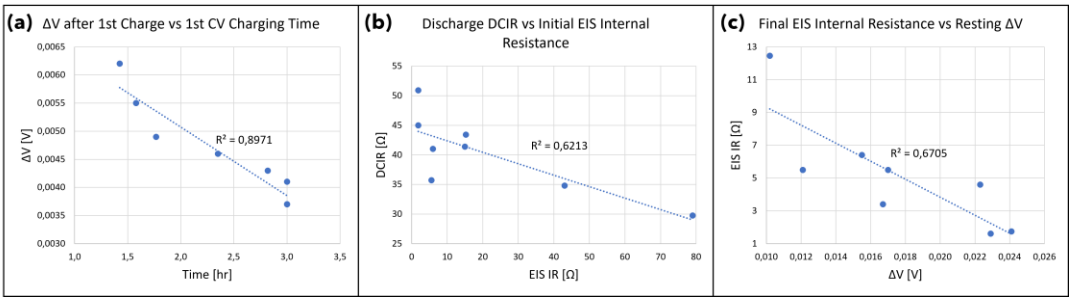

Figure 18 – Correlations between the parameters related to the 1st formation cycle.

Since only 6 cells were formed with a number of cycles higher than one, for the 2nd cycling state fewer data points were available for the study. For this state, only a relation between the median discharge voltage and the mass loading was found, presented in the graphs below (Figure 19). As can be seen, even though a clear relation is not seen if every data point is considered (Figure 19 (a)), if the one related to cell P2289 is discarded (Figure 19 (b)) the remaining points present an evident linear relation between these two parameters. One explanation for this relation is that a higher mass loading will translate in a slightly higher diffusion resistance in

the coating layer, and hence in a decrease in the median discharge voltage. However, although it would then be expected to see an increase of DCIR with mass loading for the 2nd cycling state, which would sustain this interpretation, this relation is not very clear.

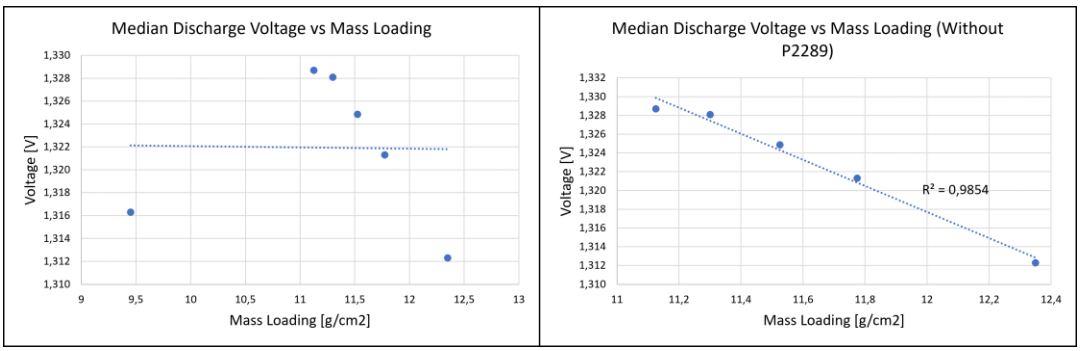

Figure 19 – Correlations between the parameters related to the 2nd formation cycle.

Similarly, since only 4 cells were formed with a number of cycles of 3 or more, no strong conclusions can be taken from the collected data for the 3rd cycling state. Nevertheless, as can be seen in the graphs below (Figure 20), a linear relation could exist between the mass loading and the discharge DCIR (as expected for the 2nd cycling state) (Figure 20 (a)) and between the mass loading and median discharge voltage (as observed for the 2nd cycling state) (Figure 20 (b)). However, more cells should be studied to verify these relations.

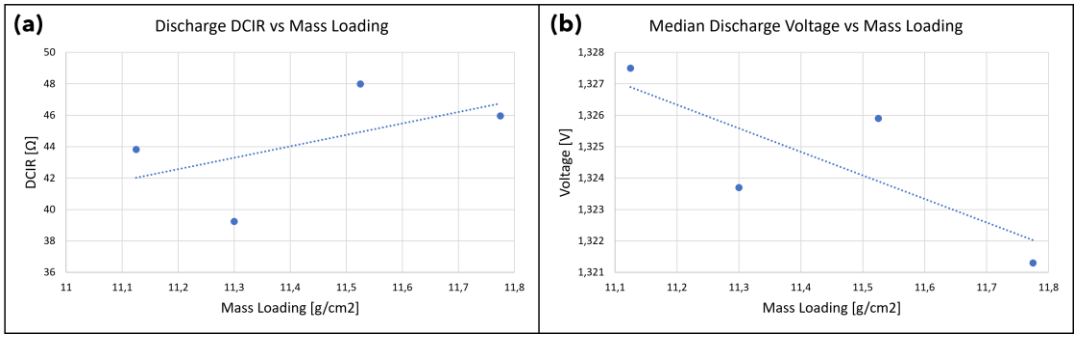

Figure 20 – Correlations between the parameters related to the 3rd formation cycle.

Lastly, as a final comment to the study of each formation cycle independently, it is worth mentioning that a linear relation was observed for every cycling state between the average and the median discharge voltage (Figure 21). Therefore, it can be concluded that the correlations found for one of them also apply for the other.

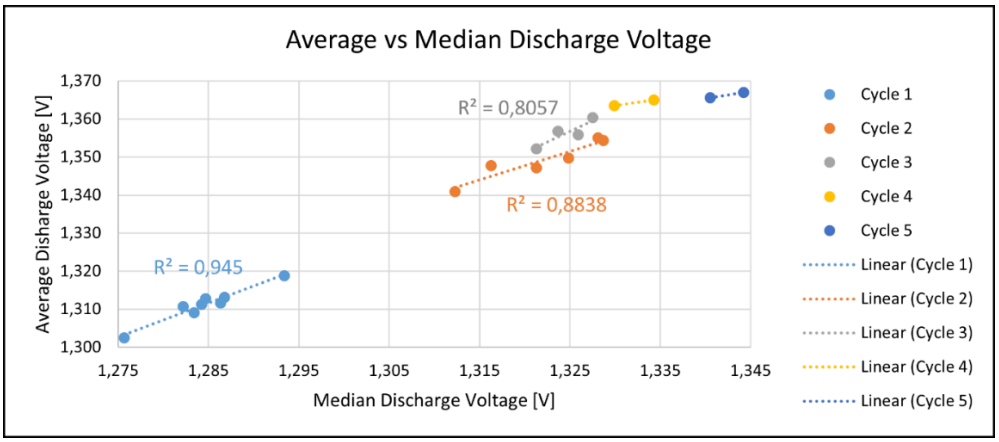

Figure 21 – Linear Relation between the average and the median discharge voltage for each cycle.

As mentioned, for a second part of the analysis, each data point was taken as an independent case, without considering from what cell or formation cycle it was retrieved. However, since, as mentioned above in Figure 17, the 1st cycle discharging profiles present a different shape (compared to the other cycles) for every cell, the data points related to this cycle were excluded from the analysis.

Even though none of the relations obtained are very clear, due mainly to the large amount of data points collected in different formation cycles, some trends were found and are presented in the graphs below (Figure 22). The discharge DCIR appears to be related to the voltage drop after the charging step, decreasing with the voltage drop increase (Figure 22 (a)). However, this contradicts what would be expected, since the voltage drop should increase for higher internal resistances, and therefore more cells should be studied to understand this relation further. Furthermore, a very rough relation was found between the discharge DCIR and the median discharge voltage (Figure 22 (b)). Since a higher internal resistance should translate in a faster discharge voltage decay, the decrease of the median discharge voltage with the increase of the discharge DCIR is coherent. Lastly, the discharge capacity seems to decrease with the median discharge voltage (Figure 22 (c)). This could be explained by the fact that a lower discharge capacity will translate into a shorter discharging curve, which will lead to a higher median discharge voltage.

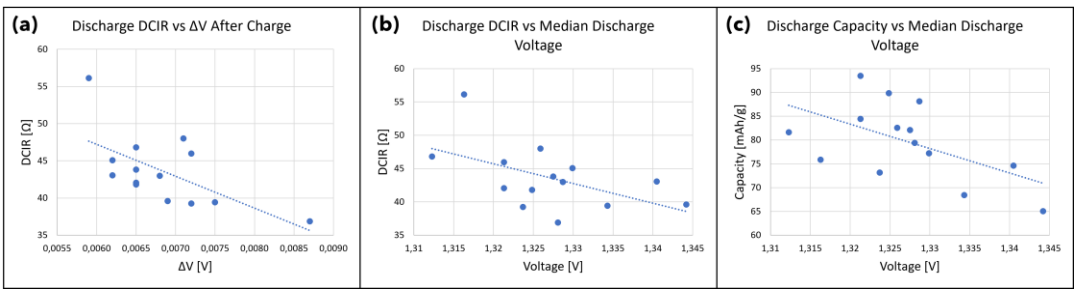

Figure 22 – Correlations between the formation cycles parameters using every data point.

By combining the results of Figure 22 (b) and (c), one would expect to see a relation between the discharge DCIR and the discharge capacity. However, this could not be read on the data collected. Moreover, a relation should also be observed associating the discharge capacity with the voltage drop after the charging step due to the trend seen in Figure 22 (a).

In order to further study these possible relations, instead of using the discharge capacity, the capacity retention between each cycle and the 1st formation cycle was calculated and evaluated. As can be noticed in the graphs below (Figure 23), no clear trend can be concluded from the data points for both the relation with the voltage drop after the charging step (Figure 23 (a)) and the discharge DCIR (Figure 23 (b)), due to a large dispersity between the collected values.

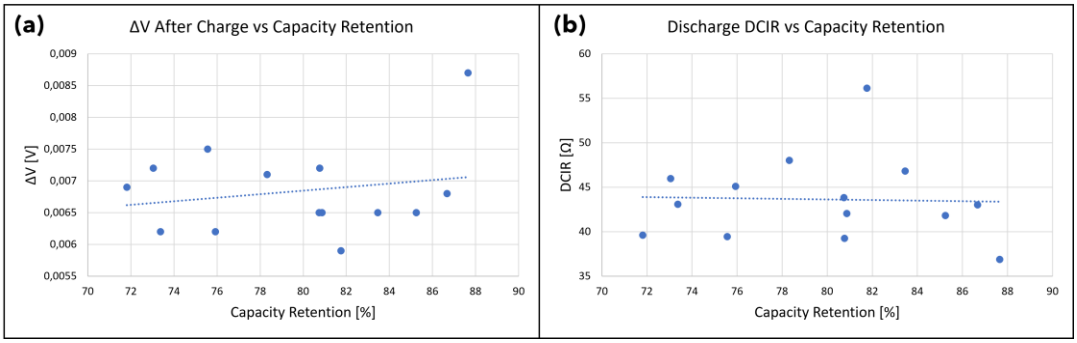

Figure 23– Correlation between the formation cycles parameters and capacity retention.

As mentioned, one of the goals of this primary study was understanding if any correlations existed between the formation cycles parameters (presented in Table 4), in order to reduce the amount of data needed to collect in future tests. On one hand, due to the graph presented in Figure 18 (a), which shows a clear linear relation between the voltage drop after the charging step and the first CV charging step time, it was concluded that in subsequent analysis this later parameter does not have to be considered, since it will present the same relations as the former. Moreover, the same conclusion was reached considering the average and median discharge voltage, which also present an apparent linear relation (Figure 21). Therefore, for the remaining tests only the median discharge voltage will be analysed.

On another hand, the final EIS internal resistance measurement will be discarded from the protocol, since it not only presented dispersed non-coherent values, but also less information compared to the discharge DCIR. Moreover, for the same reasons, the initial EIS internal resistance measurement will be replaced by an insulation test, only to guarantee no short-circuits exist in the cell before formation.

The discharge capacity will continue to be measured and used not only to filter out faulty cells but also for the calculation of the capacity retention of each cell during the cycle life tests and at the end of the self-discharge tests. By normalizing the capacity, using instead capacity retention, the comparison between cells should become more evident. Additionally, the voltage drop after the charging step and the discharge DCIR will continue to be evaluated, since several trends were related to them.

Finally, it was decided to keep the resting voltage drop and the mass loading in future studies. Even though the first parameter may not present any use for predicting the cycling life, it could be beneficial for discarding malfunctioning cells in the grading process. If an unexpected large value of the resting voltage drop occurs, this could indicate a problem in the functioning of the cell. Furthermore, the mass loading is the only parameter that could internally influence the diffusion behaviour inside the cell. However, as the manufacturing process evolves, a consistent cathodic mass loading should be reached, and hence this parameter discarded.

In conclusion, the 6 formation cycle parameters that are going to be used in future studies are presented in the table below:

Table 5– Formation cycle parameters evaluated in future studies.

Initial State	**Cycling State**
Resting Voltage Drop	Voltage Drop After Charge
Mass Loading	Median Discharge Voltage
-	Discharge DCIR
-	Discharge Capacity

Using these parameters, a final evaluation was made to understand how the cycling state collected data varied with the formation cycle number. In Figure 24, the graphs of the evolution of the voltage drop after charging (a), the median discharge voltage (b), the discharge DCIR (c), and the discharge capacity (d) as a function of the cycle number are presented. As it would be expected the discharge capacity slightly decreases with the number of formation cycles, tending to a more constant value as the cycle number increases.

However, it was observed that the values of the first 3 parameters start to become approximately constant from the 2nd cycle forward. In fact, while the values related to the 1st cycle show a high discrepancy to the rest of the collected data points for the remaining cycles, afterwards the parameters seem to have reached a practically stable state. This could also be associated to the already mentioned different shape that the 1st discharge curve presents from the rest.

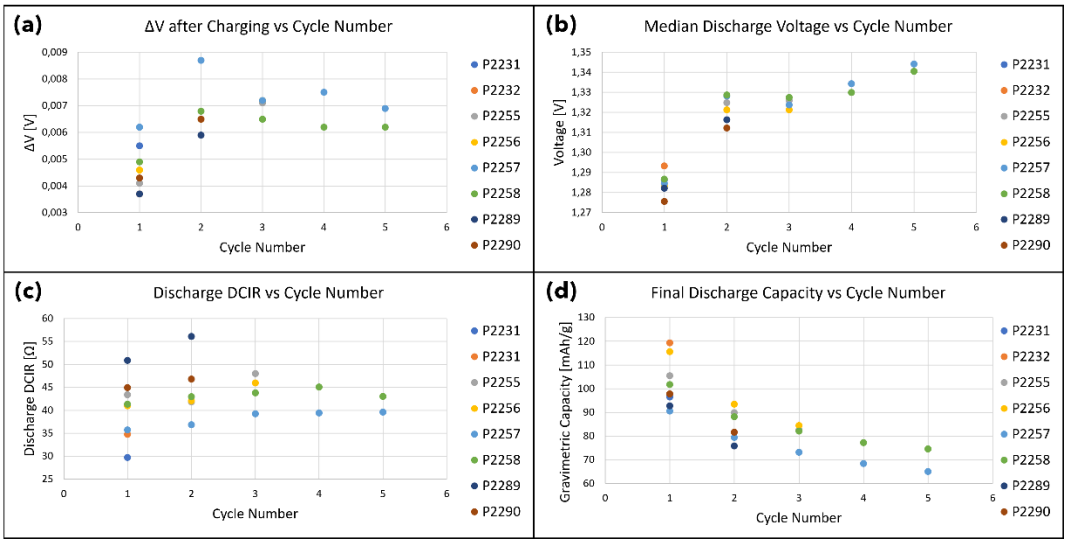

Figure 24 – Formation cycle parameters as a function of the cycle number.

5.1.3 Self-Discharge Curves Study

In order to understand if the cause of the voltage drop that creates the 2-plateau self-discharge curve was due to the cells not being fully formed, after formation the cells were left resting while connected to the cycler. While 6 of the cells were stopped after 2 weeks, cell P2231 and cell P2290 were left to self-discharge for 4. This is done to understand when the OCV would stop decaying, since for 2 weeks a positive (although very low) self-discharge rate was still observed.

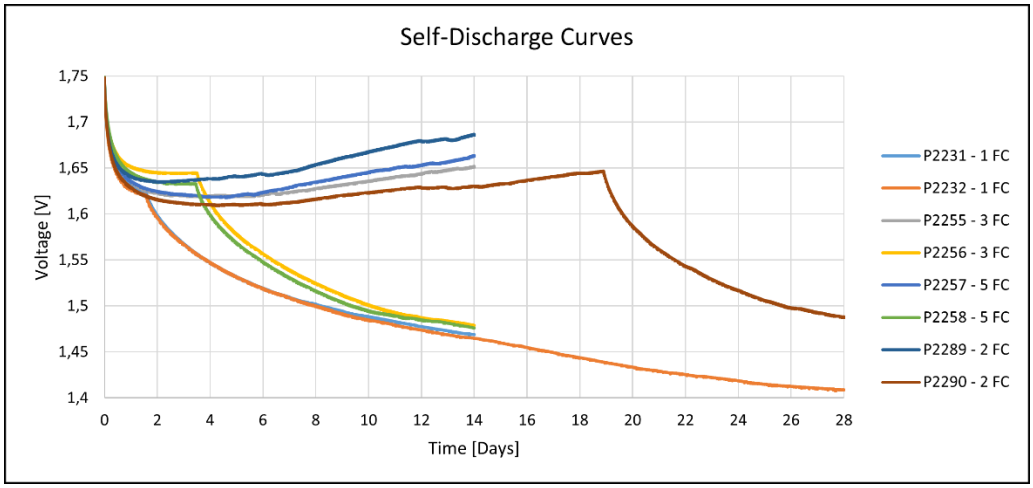

Figure 25– Self-discharge curve for the 8 cells formed with different number of formation cycles.

The first thing that can be noticed is that 4 cells (P2255, P2257, P2289, and P2290) present a very different self-discharge curve from the rest of the cells. Even though in the initial resting days the OCV seems to follow the same trend as the other cells, the curves end up hitting a voltage minimum between the 2nd and 5th self-discharge

day. Afterwards, an unexpected increase in their voltage is observed, reaching at the end of the 14-day period a much higher voltage compared to the minimum voltage. Since it is unlikely that a normal cell can even show an increase in voltage without connecting to a power source, it was therefore concluded that there had to be a current leakage on the cycler channels when these cells were tested. Consequently, these channels were re-tested using different cells, which revealed the same problem. Therefore, the channels were considered faulty and were discarded for the future tests.

Moreover, for the cells P2256 and P2258, which presented a 2-plateau self-discharge curve, the time when the voltage drop occurs is the same, similarly to what was seen in the primary testing. This information, combined with the current leakage problem seen for the 4 channels in which the cells were being charged instead of rested, supports the hypotheses that a malfunction of the cycler, resulting in undesired current leakage, could be a justification for the sudden voltage drop.

Nevertheless, with the data collected for the four 2-plateau cells, which present different formation cycles between themselves (1, 3 or 5), it was possible to assess the main purpose of this study and conclude that the number of formation cycles does not influence the existence of the voltage drop that creates the 2-plateau self-discharge curves. This conclusion not only led to further testing to try and explain this phenomenon (results presented in the following sections), but also posed the question of how many formation cycles should be used to form the fresh cells for the remaining tests.

As mentioned in the study of the formation cycle parameters as a function of the cycle number, it was seen that the data points start stabilizing after the 2nd cycle. Furthermore, when comparing the cycling curves, the charge and discharge curves related to the 1st formation cycle present a different shape from the ones from the 2nd cycle. Contrarily, the 2nd cycle curves look very similar to the 3rd, 4th, and 5th formation profiles. This means that only from the 2nd cycle forward could the formation cycle parameters mentioned above reliably be assessed and used for grading. Lastly, one last factor to consider is that higher the number of formation cycles, higher the electricity spent in forming the cells, and therefore higher the cost for the company. Due to all these reasons, for the remaining of the tests, a standard formation cycle protocol for activating the fresh cells with only two cycles was established.

5.2 Self-Discharge with Different Cathodic Current Collector

In order to verify if the voltage drop which creates the second plateau during self-discharging tests occurs due to a parasitic reaction possibly with the current collector, 2 cells were assembled using stainless steel instead of graphite paper as the cathodic current collector. The cells were formed and self-discharged for 2 weeks using the protocol in Table 2. The graph below presents the self-discharge curves of both cells.

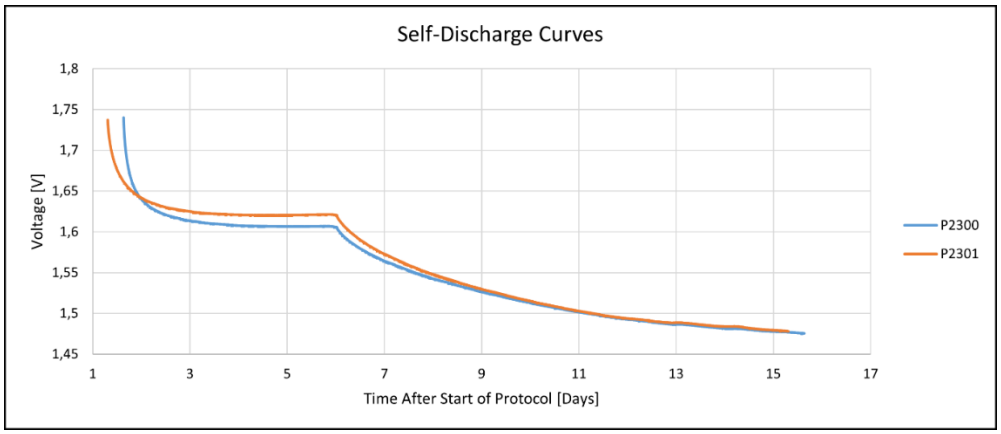

Figure 26 – Self-discharge curves for both cells using stainless steel as a cathodic current collector.

As can be verified by the 2-plateau curves above, the voltage drop is not dependent on the material of the current collector, occurring for both graphite paper and stainless steel, which indicates that no parasitic reactions with this component are related to this phenomenon.

Furthermore, since the graph of Figure 26 presents on the x-axis the time after the start of the protocol (which was started simultaneously for both cells), it was again seen that this voltage drop was occurring exactly at the same moment for both cells. Therefore, this could again sustain the argument that a momentaneous current leakage from all channels of the cycler could be the reason for these 2-plateau voltage features during self-discharging tests.

5.3 Self-Discharge due to Current Leakage Problem from the Cycler

As has been seen in the previous tests, the cells with a 2-plateau self-discharge curve presented the voltage drop at the same instant. This phenomenon could then be explained by a malfunctioning in the cycler, which would result in a simultaneous current leakage in every channel for a small time period. This leakage would be at the anode terminal, leading to a brief discharge of the cell, and therefore a sudden decrease of its voltage.

As a way of testing the cycler, 9 cells were assembled, attached to different channels, formed, and left to self-discharge, with all experiments starting at the same time. As can be seen in the graph below, all the cells present the voltage drop exactly at the same moment, after approximately 4.7 days. Therefore, it was concluded that the cycler was malfunctioning, leaking current unexpectedly, and this was considered when designing the rest of the performed tests.

Looking at the curves presented in Figure 27, even though all cells present the voltage drop at the same time, actually, none start the self-discharging process simultaneously, due to all being cycled with the same protocol but each presenting

different 1st CV charging times (related to the initial pre-formation status of each cell). This further highlights that this sudden voltage drops happening on all cells after around 4.7 days was due to the power failure of the whole instrument at a particular moment.

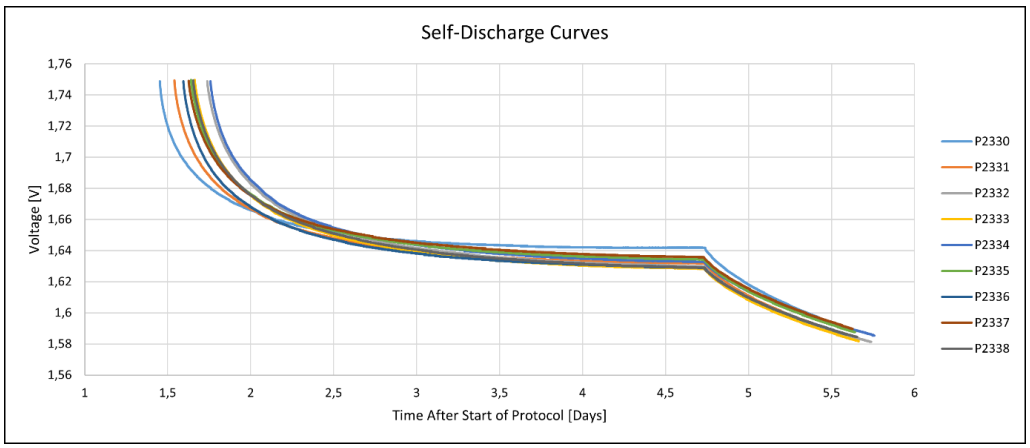

Figure 27 – Self-discharge curves for 9 cells as a means of testing the cycler.

6 Self-Discharge Tests

6.1 Methodology and Protocol

Since one of the aims of the thesis was to establish a correlation between the self-discharge mechanism of the cell and its cycling life, by trying to correlate the parameters associated with both these protocol parts, further self-discharge tests were performed. Therefore, 12 cells were submitted to additional tests – 2 being connected to a non-faulty cycler and 10 being rested for a much shorter period to try to avoid the faulty cycler's problems.

Below, the protocol used for these tests is presented. The cells were formed with the previously established 2 formation cycles, and afterwards charged and left to rest for the desired self-discharge duration. Lastly, a final discharge and DCIR discharge were carried out to obtain the cell's final capacity and internal resistance.

Table 6 – Protocol used for the self-discharge tests.

Cycling Part	Step Number	Step Name	Step Time	Voltage Limit [V]	Current Density [mA/g]	Cut-off Current [mA]	Time Record [s]
Insulation Testing	1	-					
Formation Cycles	2	Rest	12 hr	-	-	-	30 sec
	3	CC Charge	-	1.75	20	-	10 sec
	4	CV Charge	3 hr	1.75	20	0.01	10 sec
	5	Rest	10 min	-	-	-	30 sec
	6	CC Discharge	-	1.15	20	-	10 sec
	7	CC DCIR Discharge	3 sec	-	60	-	0.1 sec
	8	Cycle	Start Step: 3 Cycle Count: 2				
Self-Discharge Test	10	Rest	10 min	-	-	-	30 sec
	11	CC Charge	-	1.75	20	-	10 sec
	12	CV Charge	3 hr	1.75	20	0.01	10 sec
	13	Rest Self-Discharge	Self-Discharge Time	-	-	-	30 sec

	14	CC Discharge	-	1.15	20	-	10 sec
	15	CC DCIR Discharge	3 sec	-	60	-	0.1 sec
End	16	-					

Since, as mentioned in the previous section, the cycler available for testing is faulty, presenting unpredictable current leakage to the cells' terminals, the duration of the self-discharge tests had to be substantially decreased from the initially intended 2 weeks to 3 days. By decreasing the testing time, the intent was to avoid a high current leakage from the cycler, finishing the resting period before the formerly seen high voltage drop, and thus obtaining a 1-plateau self-discharge curve. Moreover, stopping the resting period before the high voltage drop was necessary to be able to obtain a correct value for the final capacity and DCIR after self-discharge.

Nevertheless, in order to not only study a longer self-discharge but also ensure that the 1-plateau curve is in fact the correct one, 2 cells were left to self-discharge for 2 weeks in another non-faulty smaller cycler.

6.2 2-Week Self-Discharge Tests

The graph below shows the 2-week self-discharge curves obtained from the non-faulty cycler. These tests confirmed that the correct shape of these curves only presents 1 plateau, as seen in the literature. Moreover, this confirmed the conclusion drawn in the previous section that the cycler used for the rest of the cells' testing is faulty, leaking current unpredictably.

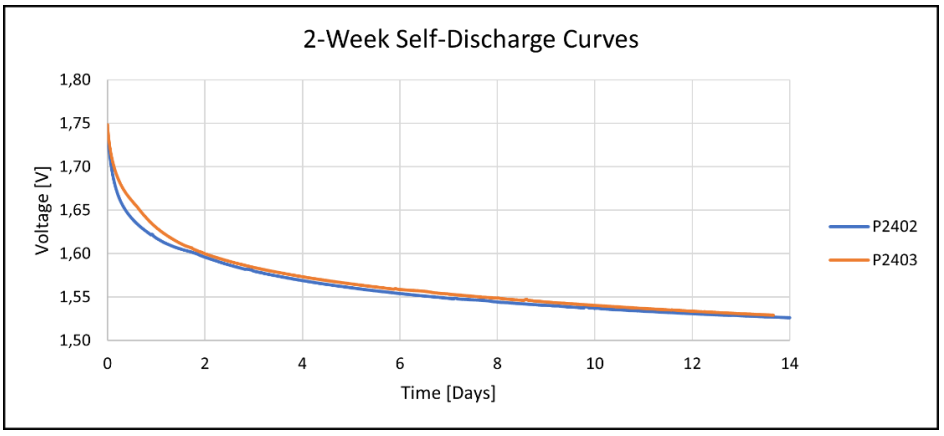

Figure 28 – 2-week self-discharge curves obtained from the non-faulty cycler.

6.3 3-Day Self-Discharge Tests

Having finally understood that a 1-plateau curve is the correct representation of the self-discharge mechanism, 10 cells were left to self-discharge for a resting period of 3 days. It is worth noticing that these 10 cells were the same that were previously left to self-discharge for a longer period, in order to study the voltage drop that created the 2-plateau curve (Figure 27). Therefore, the complete protocol that these cells have been through was:

1. 2 Formation Cycles;
2. Self-Discharge Test for approximately 6 days (until a high voltage drop was observed);
3. 1 cycle between self-discharge tests to obtain relevant data parameters;
4. Self-Discharge Test for 3 days (to get a 1-plateau curve).

Below, the 3-day self-discharge curves of the 10 cells are presented.

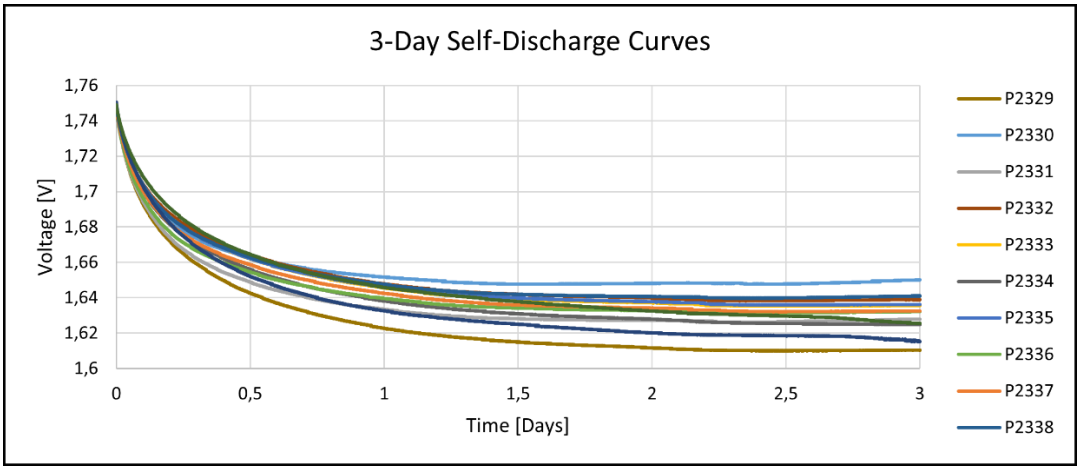

Figure 29 – 3-day self-discharge curves.

As can be observed, by decreasing the resting time from 2 weeks to 3 days, it was possible to avoid a high current leakage from the cycler, thus obtaining a 1-plateau curve for every cell. However, this does not imply that no current leakage influenced the results. As can be verified from, for example, the curve associated to cell P2330, an increase in the voltage around the 2.8 day confirms that a small current leakage from the cycler charged the cell. Therefore, even though a high current leakage was in fact averted by decreasing the resting time, small unknown leakages from the cycler cause the obtained data to not be very reliable.

When analysing the 2-week curves presented in the previous section, it can be read that the voltage drop for the first 3 days is approximately 0.18 V. Nevertheless, for the 3-day self-discharge, the 10 cells present an average value for the voltage drop around 0.12V. This much lower value seems strange considering that the 10 cells have undergone a much longer protocol, being therefore more aged, which should translate into a higher self-discharge rate. Assuming that the data related to the 2-week self-discharge is the correct one, the justification for these inconsistent results

could once again be related to the faulty cycler. As mentioned above, it is possible that, from the beginning of the resting period, a very small current leakage from the cycler is entering the terminals, slightly charging the cell, and opposing the self-discharge mechanisms. For this reason, what is actually seen in the 3-days data is not only a result of the cells' self-discharge, but actually a combination of these processes with a small voltage increase due to charging from the cycler. Thus, the voltage drop for these curves appears to be much lower than it is in reality.

This new understanding of the self-discharge data could lead to a re-interpretation of the 2-plateau curves. Contrarily from what was stated in the previous section, the voltage drop that creates the 2 plateaus could be unrelated to a high current leakage but instead be associated with the end of this current leakage. If, for a small period, the cycler stops leaking current that is charging the cells, these will enter a relaxation process, decreasing voltage at a higher rate, which could be the reasoning for the high voltage drop.

Although there is no way of truly understanding what is actually happening inside the cycler, from the graph presented in Figure 29 it is very clear that it affects the results obtained. For this reason, even though, on a first instance, the intent of these tests was to associate the self-discharge mechanism with the formation cycles, any correlations found between the related parameters would not be trustworthy. Furthermore, the same could be stated if any correlation was found between the self-discharge and the cycle life results. For this reason, since no reliable conclusions could be reached from this data, no further analysis will be performed using the parameters related to these self-discharge tests. Nevertheless, for future research, understanding not only the relation between formation cycles and self-discharge but also how the latter influences the cycling life of a battery cell, by running several tests in a non-faulty cycler, could be of great interest.

7 Cycle Life Tests

7.1 Methodology and Protocol

The main goal of this thesis was to find and establish a grading and quality control system for zinc-ion battery cells. Through the study of the relation between manufacturing and formation of these cells and their cycling life performance, a quality control procedure could be instituted at the company to guarantee that only good cells reach the customer. Therefore, this procedure must be capable of being integrated in the manufacturing and formation processes, since these are the parts performed at the company.

For this purpose, it is necessary to understand what constitutes a good and a bad cell and correlate these definitions with the previously collected formation cycle parameters. In other words, the grading of the cells as good or bad should be able to be performed by looking at the parameters from the formation cycles before delivering the cells to the customers. To achieve this, several cells were formed, submitted to long cycle life tests, and then evaluated based on their performance.

The protocol for the cycle life tests is presented in the table below. As can be seen, the cells are first formed with 2 formation cycles based on the previous conclusion in chapter 5.1.3. The life cycle part is done as follows: 2 slow cycles (using a current density of 10 mA/g) are performed every 10 fast cycles (with current density 40 mA/g). While the slow cycles (designated validation cycles) are used to retrieve the correct values of the desired cycle life parameters, the fast cycles (designated ageing cycles) are performed to age the cell in a faster way. As mentioned previously, the reason why 2 validation cycles are used instead of only one is due to the cells' memory effect. Every cycle is constituted by a CC followed by a CV charge until a voltage of 1.75 V, a CC discharge to a voltage of 1.15 V (where the capacity is also read), and lastly a fast CC discharge (with a current density of 60 mA/g) in order to obtain the DC internal resistance value.

Table 7 – Protocol used for the cycle life tests.

Cycling Part	Step Number	Step Name	Step Time	Voltage Limit [V]	Current Density [mA/g]	Cut-off Current [mA]	Time Record [s]
Insulation Testing	1	-					
Formation Cycles	2	Rest	12 hr	-	-	-	30 sec
	3	CC Charge	-	1.75	20	-	10 sec
	4	CV Charge	3 hr	1.75	20	0.01	10 sec
	5	Rest	10 min	-	-	-	30 sec

	6	CC Discharge	-	1.15	20	-	10 sec
	7	CC DCIR Discharge	3 sec	-	60	-	0.1 sec
	8	Cycle	Start Step: 3 Cycle Count: 2				
Cycle Life Tests	9	Rest	10 min	-	-	-	30 sec
	10	CC Charge	-	1.75	10	-	10 sec
	11	CV Charge	3 hr	1.75	10	0.01	10 sec
	12	Rest	10 min	-	-	-	30 sec
	13	CC Discharge	-	1.15	10	-	10 sec
	14	CC DCIR Discharge	3 sec	-	60	-	0.1 sec
	15	Cycle	Start Step: 9 Cycle Count: 2				
	16	CC Charge	-	1.75	40	-	10 sec
	17	CV Charge	3 hr	1.75	40	0.01	10 sec
	18	Rest	10 min	-	-	-	30 sec
	19	CC Discharge	-	1.15	40	-	10 sec
	20	Cycle	Start Step: 16 Cycle Count: 10				
	21	Cycle	Start Step: 9 Cycle Count: Depends on Dataset				
	22	CC Charge	-	1.75	10		10 sec
	23	CV Charge	3 hr	1.75	10	0.01	10 sec

	24	Rest	10 min	-	-	-	30 sec
	25	CC Discharge	-	1.15	10	-	10 sec
	26	CC DCIR Discharge	3 sec	-	60	-	0.1 sec
	27	Cycle	Start Step: 22 Cycle Count: 2				
End	28	-					

In order to study the cells cycling behaviour at different conditions, 3 different groups of cells were submitted to these tests, resulting in 3 different datasets:

- Room Temperature Dataset – cycle life tests were performed for 10 cells at room temperature. These cells were the same 10 cells which had been previously tested for self-discharge (see previous section) and were therefore more aged than the cells that constitute the other datasets.
- 25°C Dataset – using an environmental chamber, 10 cells were formed and tested at 25°C.
- 5°C Dataset – using an environmental chamber, 10 cells were tested at 5°C. Nevertheless, in order to compare the results with the previous dataset, the temperature was only changed for the cycle life part, and these cells were also formed at 25°C.

7.2 Cycle Life Data Analysis Method

For each dataset, the data analysis related to the cycle life tests is divided into 3 parts (Figure 30). On a first instance, by looking at the parameters collected in the validation cycles, each cell is studied individually to understand if it should be included or discarded from the rest of the analysis. Afterwards, the remaining cells are divided into 2 groups – as good or bad cells - depending on their behaviour (quantified by their capacity retention) at the end of life. Lastly, correlations are studied between the formation cycle parameters and the good or bad status previously attributed to each cell.

The purpose of the first step is to understand if the cell behaved properly until the end of the cycle life tests, or if it was influenced by external factors (as electrolyte drying or coating delamination), resulting in unreliable results, and thus being excluded from the analysis. To this goal, several parameters – such as the discharge capacity, the coulombic efficiency, the median discharge voltage, the capacity retention, and the discharge DCIR – were evaluated for the validation cycles. Among these parameters, it was seen that looking at the discharge capacity and DCIR was

enough to primarily filter out these cells from further analysis, since usually a low capacity and or a high DCIR is obviously a good indication of bad cells.

In the second step, the capacity retention data for the end-of-life (last validation cycle) was used to divide the rest of the cells into good or bad cells. By studying each dataset's cells together, it was possible to define capacity retention thresholds that allowed this division to be performed. Once a threshold was defined, the cells that showed a capacity retention value for the last validation cycle higher than the threshold were considered as good cells, and the ones that showed a lower value as bad cells. A fundamental mindset to select a proper threshold was to always guarantee that there were at least 2 good and 2 bad cells. Since different datasets presented cells with different end-of-life capacity retentions, the values of the defined thresholds varied between sets.

Lastly, in the third step, correlations were studied between the formation cycles and the good or bad cell status. In order to accomplish this, a correlation matrix was built for each dataset, associating the formation cycle parameters with the good (for which was attributed a positive integer) or bad (negative integer) behaviour of the cell. A correlation matrix summarizes the correlations within a dataset, by displaying the correlation parameters for different variables [82].

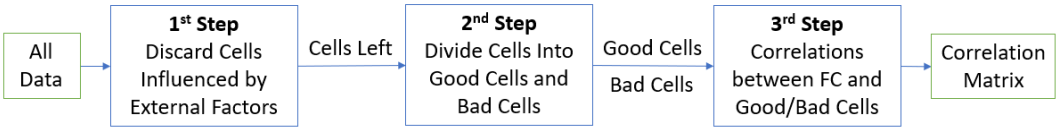

Figure 30 – Cycle life data analysis method.

7.3 Room Temperature Dataset

As mentioned above, the 10 cells that went through the self-discharge tests presented in the previous section were further studied, being submitted to cycle life tests at room temperature. Since these cells had already been tested for longer than 1 month, it is worth noticing that external factors, as electrolyte drying or coating delamination, could become more influential for this dataset.

The evolution of the cells' internal resistance (Figure 31 (a)) and of the cells' discharge capacity (Figure 31 (b)) as a function of the cycle number is shown below. For each cell, the graphs present only the datapoints related to every second validation cycles. As can be clearly seen, for 4 of the 10 cells, a very fast increase of the internal resistance is observed, which is a consequence of electrolyte drying inside the cell. Furthermore, by comparing both graphs, it can be noticed that the same 4 cells present a much higher decrease in discharge capacity compared to the other ones, which is coherent. For these reasons, the data related to cells P2329, P2332, P2333, and P2338 was discarded from the rest of the analysis.

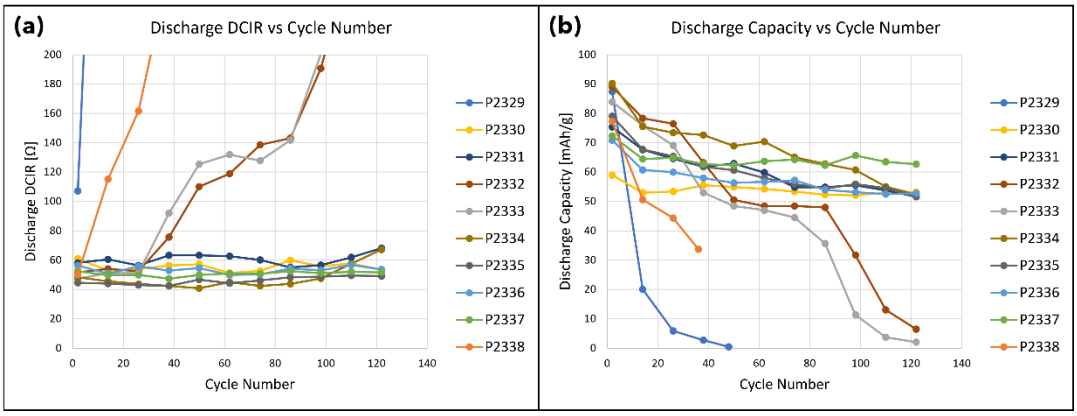

Figure 31 – Discharge DCIR and capacity as a function of cycle number for the room temperature dataset.

In order to grade the remaining 6 cells as good or bad, 3 capacity retention thresholds were defined. These were chosen based on the datapoints shown in Figure 32, guaranteeing that for each threshold there were always at least 2 good (capacity retention of the last cycle higher than the limit) and 2 bad (capacity retention of the last cycle lower than the limit) cells. The thresholds used were: 66%, 70%, and 75%.

Looking at the graph presented in Figure 32, two cells clearly stand apart, presenting a very stable cycling life with a very high capacity retention at the end of the protocol – cells P2330 and P2337. This stable performance is even more impressive considering that these cells have already been cycling for over one month (since before they were submitted to the self-discharge protocol). Hence, this is a distinct indication that a very stable cell can in fact be achieved for this chemistry. Furthermore, it implies that the degradation effects seen in other cells could just be related to external failures, such as electrolyte drying or coating delamination, resulting from the assembly process. These observations will be addressed further below.

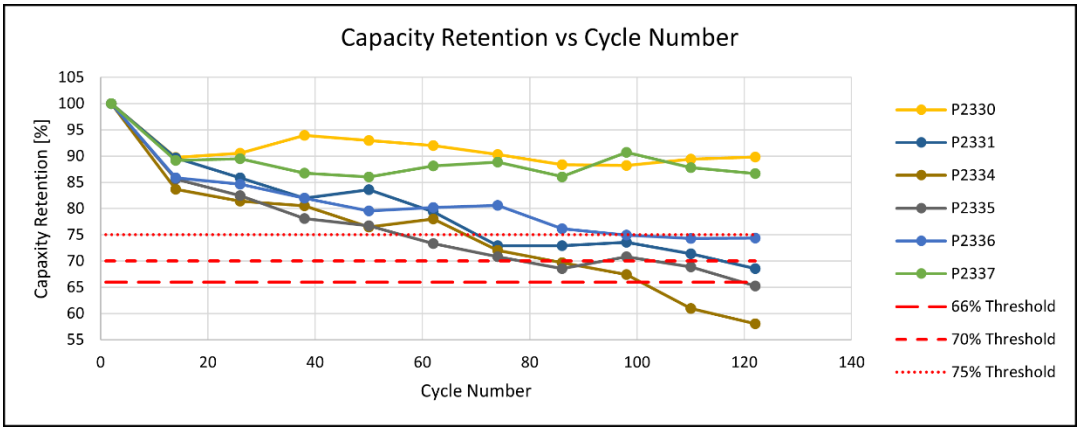

Figure 32 – Capacity retention as a function of cycle number for the room temperature dataset.

Having divided the remaining 6 cells into good and bad for each threshold, a correlation matrix was done to verify if any formation cycle parameters could predict the behaviour of the cell. In order to do so a positive value was attributed to the good cells, and a negative value to the bad cells. Below, the correlation matrix for the room temperature dataset is presented. The parameters studied are related to the 1st and 2nd formation cycle, and to the cycle performed between the 2 self-discharge tests that these cells have been submitted to (see previous section). A strong correlation is assumed to exist if the value in the matrix is above 0.75 (or lower than -0.75).

Correlation Matrix - Room Temperature Dataset				
	Parameter	66% Threshold	70% Threshold	75% Threshold
	Mass Loading [mg/cm2]	-0,19	0,24	0,01
1st FC	ΔV After Charging [V]	0,86	0,79	0,62
	Median Dch Voltage [V]	-0,69	-0,45	-0,57
	FC DCIR [Ω]	0,32	-0,43	-0,22
	FC Capacity [mAh/g]	-0,51	-0,41	-0,62
2nd FC	ΔV After Charging [V]	0,71	0,49	0,28
	Median Dch Voltage [V]	-0,56	-0,31	-0,40
	FC DCIR [Ω]	0,78	0,36	0,52
	FC Capacity [mAh/g]	-0,70	-0,52	-0,60
Parameters Cycle Before SD	ΔV After Charging [V]	0,75	0,63	0,67
	Median Dch Voltage [V]	-0,66	-0,37	-0,26
	FC DCIR [Ω]	0,94	0,44	0,34
	FC Capacity [mAh/g]	-0,66	-0,62	-0,67

Figure 33 – Correlation matrix for the room temperature dataset.

The first important result found for the room temperature dataset, which can be observed in the matrix presented, is that no parameter presents a strong correlation for the 3 thresholds. Moreover, for different thresholds, correlations with different parameters were found. While for the 66% threshold (which presents 4 good and 2 bad cells) many parameters seem to be related to the good/bad performance, for the 70% (3 good and 3 bad cells) or 75% (2 good and 4 bad cells) thresholds few or none, respectively, have any correlation.

For this reason, since no parameter presents a strong relation for every threshold, no conclusion can be taken with certainty from this dataset. A clear reason for this could be the very low number of datapoints used for the analysis. Increasing the number of tested cells in future research could lead to stronger or even new correlations, enabling to get a better insight of what formation cycle parameters can be used to predict good and bad cell performance.

In order to understand better the analysis done in the correlation matrix, the graph showing the relation between the 1st formation cycle voltage drop after charging and the good or bad definition of the cell is presented below. As mentioned, the good or bad status is represented by attributing to the good cells a positive integer (if their final capacity retention is above the threshold) and to the bad cells a negative integer (if their capacity retention is below the threshold). In Figure 34, for better visualization, different pairs of opposite numbers are chosen for distinct thresholds.

It is seen that, for the 2 lower thresholds, the cell behaves poorly if the 1st formation cycle voltage drop after charging is below a certain value, and well if it is above. Therefore, since there seems to be a clear voltage drop value that separates the good and bad cells, the correlation matrix shows a strong correlation number for this parameter for these 2 thresholds. However, for the 75% threshold, no voltage drop value can divide the good and bad cells, which leads to a not strong correlation number in the matrix.

Since a higher voltage drop is usually associated with a higher internal resistance, a possible explanation for this correlation could be associated with the formation of the ZHS layer during the formation cycles. If the ZHS layer can be properly formed after the 1st cycle, thus the cell presenting higher internal resistance and higher voltage drop after charging, this could translate into a good behaviour of the cell. Nevertheless, as mentioned before, since this correlation is not present for the 3 thresholds, no strong conclusions can be reached.

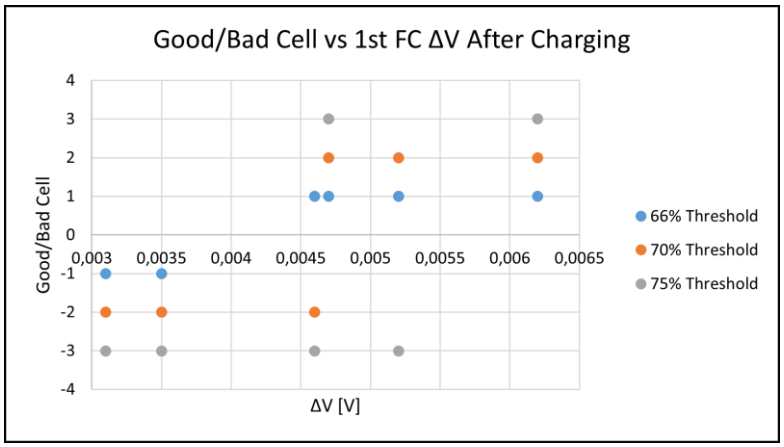

Figure 34 – Good (positive value) or bad (negative value) behaviour of the cell as a function of the 1st formation cycle voltage drop after charging for the 3 chosen thresholds.

7.4 25°C Dataset

Using the protocol presented in Table 7, 10 cells were formed and cycled inside a temperature chamber at 25°C. As for the room temperature dataset, 4 of the 10 cells present a very high increase in internal resistance shown in Figure 35 (a), which translates into a faster decrease in the discharge capacity (capacity fading) seen in Figure 35 (b). This was once again attributed to electrolyte drying inside the cell, and, for this reason, cells P2348, P2352, P2354 and P2357 were removed from the rest of the analysis. Lastly, by comparing the graphs of Figure 35 with the ones on Figure 31, it is possible to notice that the discarded cells seem to die at later cycles for the 25°C dataset than for the room temperature dataset, which is coherent with the protocols that the cells have been submitted to. Since the room temperature cells had already been through long self-discharge tests, it would be expected that external factors, as electrolyte drying, would be more influential for this dataset.

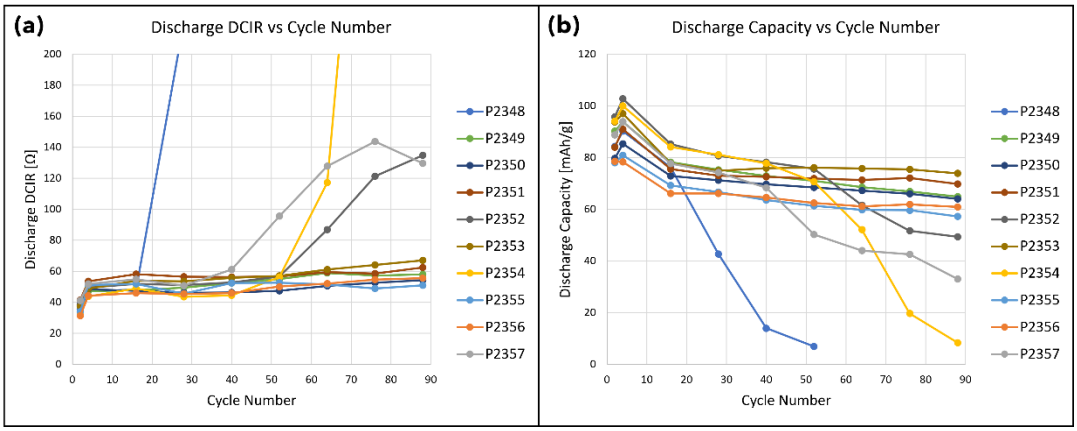

Figure 35 - Discharge DCIR and capacity as a function of cycle number for the 25°C dataset.

In Figure 36, the capacity retention data used to define the thresholds is presented. Once again, a comparison with the datapoints presented in Figure 32 shows that the cells from the 25°C dataset present higher capacity retentions values than the ones from the room temperature dataset, which can again be justified by the longer protocol that the later have been submitted to.
In order to divide the remaining 6 cells into good and bad cells, 3 capacity retention thresholds were used for the analysis: 75%, 76%, and 76.5%.

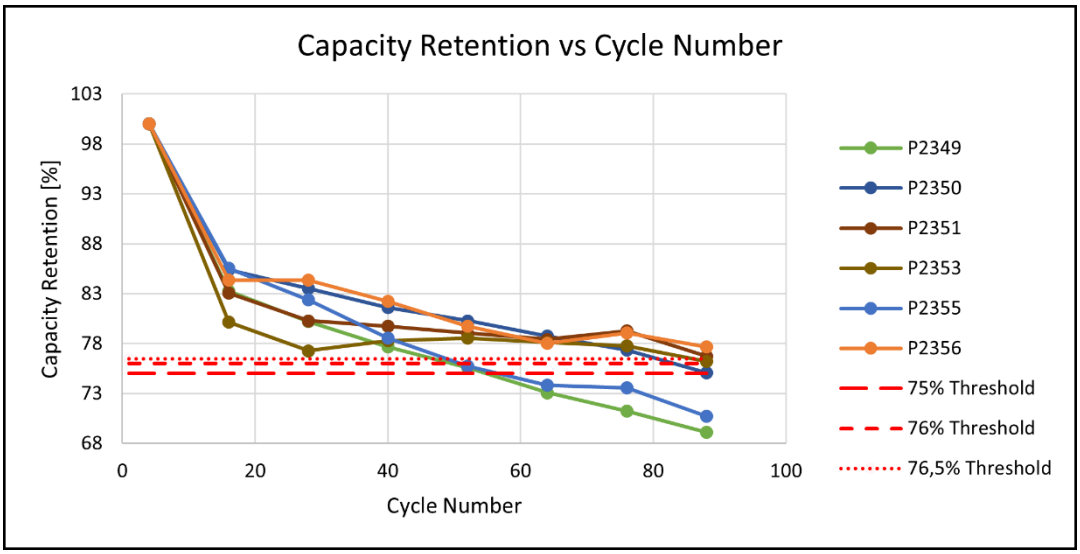

Figure 36 - Capacity retention as a function of cycle number for the 25°C dataset.

In order to verify if any correlation existed between the formation cycle parameters and the good or bad status attributed to each cell, the correlation matrix presented in Figure 37 was built. Contrarily to the matrix obtained for the room temperature dataset, even though in this study the thresholds defined are closer to each other, very few strong correlations (only one) appear. Furthermore, as seen in section 7.3,

no parameter presents a strong correlation for the 3 thresholds. As for the room temperature dataset, this could be related to the low number of datapoints used in the analysis. A larger sample could show stronger or even newer correlations. Nevertheless, with the obtained results, no strong conclusions can be drawn.

Correlation Matrix - 25°C Dataset				
	Parameter	75% Threshold	76% Threshold	76,5% Threshold
	Mass Loading [mg/cm2]	0,27	0,45	0,45
	ΔV Initial Rest [V]	-0,32	-0,29	-0,37
1st FC	ΔV After Charging [V]	0,13	0,16	0,64
	Median Dch Voltage [V]	-0,34	-0,04	-0,15
	FC DCIR [Ω]	0,77	0,38	0,01
	FC Capacity [mAh/g]	0,04	0,33	-0,04
2nd FC	ΔV After Charging [V]	0,05	-0,52	0,02
	Median Dch Voltage [V]	-0,02	0,67	0,59
	FC DCIR [Ω]	0,21	0,01	-0,06
	FC Capacity [mAh/g]	-0,01	0,24	-0,32

Figure 37 - Correlation matrix for the 25°C dataset.

As seen in the correlation matrix above, the only strong correlation found was for the internal resistance related to the 1st formation cycle. As shown in the graph below, this is due to the fact that only for the 75% threshold it is possible to find a DCIR value that divides the cells into good and bad (around 33.1 Ω).
Nevertheless, even though this correlation is not found for the other thresholds, which precludes any strong conclusions, it is worth noticing that its explanation could be connected with the results found for the room temperature dataset: a higher internal resistance could also be related with a good formation of the ZHS layer during formation cycles, which translates into a stable and good operation of the cell.

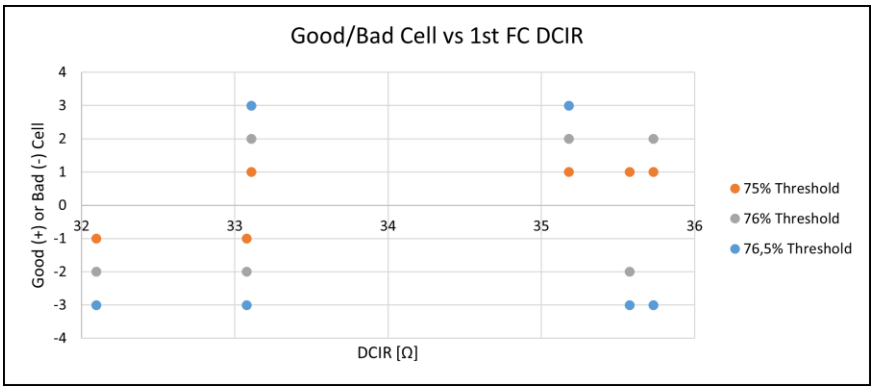

Figure 38 - Good (positive value) or bad (negative value) behaviour of the cell as a function of the 1st formation cycle DCIR for the 3 chosen thresholds.

7.5 5°C Dataset

As for the 25°C dataset, 10 cells were assembled and submitted to the protocol in Table 7 in an environmental chamber. In order to study the behaviour of the cells at different temperatures only for the cycle life part, the 10 cells were still formed at 25°C and only afterwards the temperature in the environmental chamber reduced to 5°C. This will also mimic the real-world case, where the company can only set and control the conditions during the cell formation, since the customers will decide how to use the cells at various environments.

Looking at Figure 39 (a), even though cell P2434 shows a normal internal resistance value for the 2nd formation cycle (first datapoint in the graph), when the temperature is reduced to 5°C, the DCIR values increase substantially, becoming much higher compared to the other cells. This most probably indicates that something wrong happened in the cell when changing its temperature, and thus its datapoints were removed for the remaining analysis. Furthermore, in Figure 39 (b), cell P2436 presents a much lower initial discharge capacity (for the 2nd formation cycle) compared to the others. This is an indication of a malfunction in the cell, and hence this cell was also discarded from the study.

Lastly, comparing the DCIR and discharge capacity values obtained for the cells at 5°C and 25°C, it is possible to conclude that, as seen in the literature (Figure 5 and Figure 2, respectively), the value of these parameters decrease and increase, respectively, with temperature.

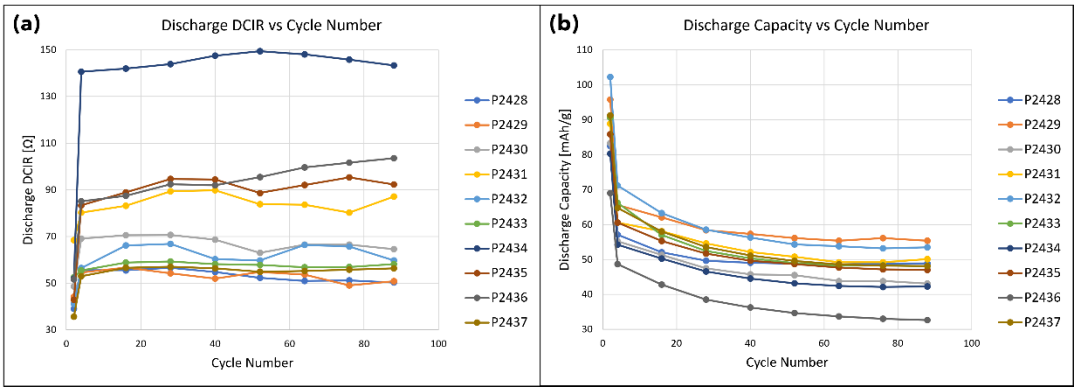

Figure 39 - Discharge DCIR and capacity as a function of cycle number for the 5°C dataset.

Since for this dataset only 2 cells were discarded from the analysis, 5 different capacity retention thresholds can be used to divide the 8 remaining cells, guaranteeing that there are always at least 2 good and 2 bad cells. Therefore, using the capacity retention values for the last validation cycle (Figure 40), the thresholds used for the analysis of this dataset were: 75%, 76%, 78%, 79%, and 83%.

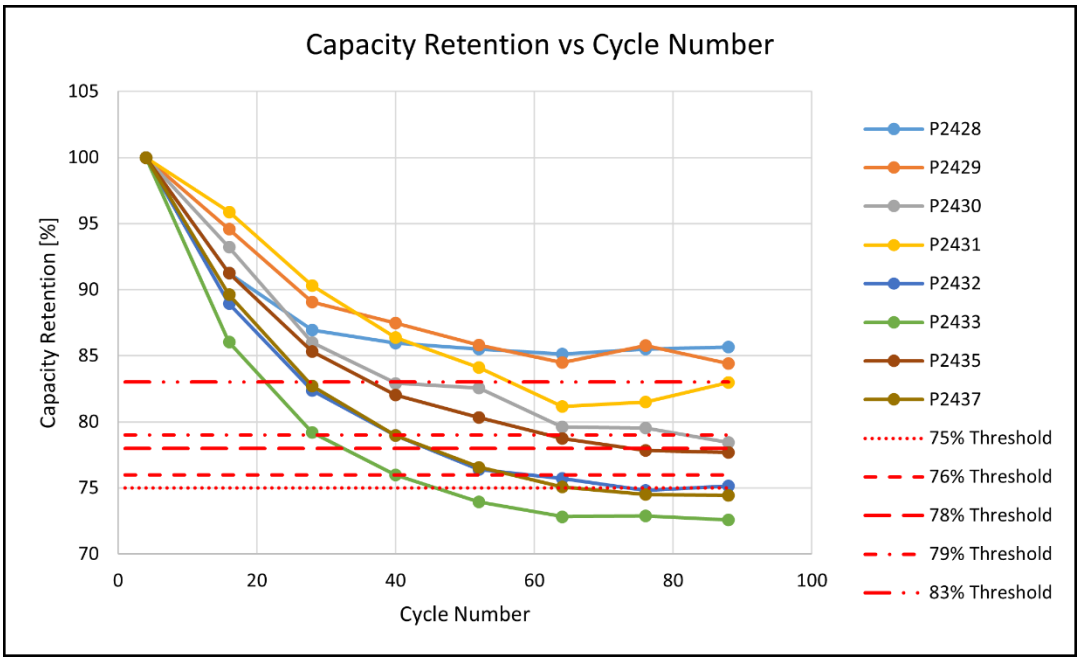

Figure 40 - Capacity retention as a function of cycle number for the 5°C dataset.

The correlation matrix for the 5°C dataset is presented in Figure 41. As can be seen, even though a larger number of datapoints and thresholds were used in this study, no parameter showed any strong correlation with the previously defined good or bad behaviour of the cell for any threshold. For the 75% and 76% thresholds, not so strong correlations were seen, but as mentioned before, increasing the sample size, and thus the number of datapoints, could lead to the strengthen of these correlations or even the appearance of new ones.

	Correlation Matrix - 5°C Dataset					
	Parameter	75% Threshold	76% Threshold	78% Threshold	79% Threshold	83% Threshold
	Mass Loading [mg/cm2]	-0,01	0,26	0,43	0,28	-0,11
	ΔV Initial Rest [V]	0,28	-0,05	-0,24	-0,20	-0,25
1st FC	ΔV After Charging [V]	-0,23	-0,17	0,07	-0,44	-0,15
	Median Dch Voltage [V]	0,03	-0,24	-0,31	-0,16	0,46
	FC DCIR [Ω]	0,22	0,25	0,34	0,31	-0,27
	FC Capacity [mAh/g]	-0,16	-0,63	-0,49	-0,20	-0,12
2nd FC	ΔV After Charging [V]	0,56	0,00	0,09	0,07	0,05
	Median Dch Voltage [V]	-0,12	-0,32	-0,46	-0,26	0,36
	FC DCIR [Ω]	0,15	0,28	0,36	0,32	-0,30
	FC Capacity [mAh/g]	-0,08	-0,58	-0,40	-0,13	-0,09

Figure 41 - Correlation matrix for the 5°C dataset.

7.6 Analysis Combining the Different Datasets

Since from the analysis of each dataset individually no parameter showed strong correlations for every threshold, the 3 datasets were combined and analysed together as a way of increasing the number of datapoints. For this study, a capacity retention threshold of 75% was chosen for being the only value for which every

dataset presented at least 2 good and 2 bad cells. Moreover, since for different datasets different parameters were evaluated (depending on the protocol the cells had been through), for this study only the common variables between datasets were used.

As can be seen in the matrix presented in Figure 42, no correlation was found between the studied parameters and the good or bad behaviour of the cells. This is mainly associated with the fact that, when using 75% capacity retention as the threshold, different datasets displayed correlations with distinct parameters. Therefore, since the strongest features vary from set to set, when combined, the correlation values cancel each other.

Correlation Matrix - All Datasets

	Parameter	75% Threshold
	Mass Loading [mg/cm2]	-0,23
1st FC	ΔV After Charging [V]	0,15
	Median Dch Voltage [V]	-0,11
	FC DCIR [Ω]	0,28
	FC Capacity [mAh/g]	-0,09
2nd FC	ΔV After Charging [V]	0,32
	Median Dch Voltage [V]	-0,13
	FC DCIR [Ω]	0,28
	FC Capacity [mAh/g]	-0,05

Figure 42 – Correlation matrix for all datasets combined.

On the other hand, since contrarily to the room temperature dataset, the 25°C and 5°C datasets presented the exact same protocol, a correlation matrix was built using the datapoints from these 2 sets. However, as can be seen in Figure 43 (a), no correlation was found between the parameters and the good or bad behaviour of the cell. Lastly, as the ambient temperature of the lab is close to 25°C, a final study was conducted combining the datapoints of the room temperature and 25°C datasets. The results are presented in the correlation matrix shown in Figure 43 (b), but no correlations were found as well.

(a) Correlation Matrix - 25°C + 5°C Datasets

	Parameter	75% Threshold
	Mass Loading [mg/cm2]	0,04
1st FC	ΔV After Charging [V]	-0,11
	Median Dch Voltage [V]	-0,07
	FC DCIR [Ω]	0,24
	FC Capacity [mAh/g]	-0,04
2nd FC	ΔV After Charging [V]	0,25
	Median Dch Voltage [V]	-0,10
	FC DCIR [Ω]	0,17
	FC Capacity [mAh/g]	0,00

(b) Correlation Matrix - Room Temperature + 25°C Datasets

	Parameter	75% Threshold
	Mass Loading [mg/cm2]	-0,11
1st FC	ΔV After Charging [V]	0,42
	Median Dch Voltage [V]	-0,15
	FC DCIR [Ω]	0,19
	FC Capacity [mAh/g]	-0,20
2nd FC	ΔV After Charging [V]	0,33
	Median Dch Voltage [V]	-0,10
	FC DCIR [Ω]	0,28
	FC Capacity [mAh/g]	-0,24

Figure 43 – Correlation matrix for the combination of the 25°C and 5°C datasets and for the combination of the room temperature and 25°C datasets.

In conclusion, these results obtained from combining datasets emphasise the already mentioned fact that no strong conclusions can be drawn about these correlations.

7.7 Slow Cycle Life Tests

As a final study, 2 cells were submitted to slow cycle life tests with a slow current density at room temperature. For this purpose, instead of following the protocol used for the previous datasets, where 10 ageing (fast) cycles were employed to boost the ageing time of the cells, these 2 cells were only cycled with a constant current density of 10 mA/g.

Below, the testing protocol is presented. As can be seen, the cells are formed with the usual 2 formation cycles and then slow cycled for 83 cycles, being obtained the internal resistance for each cycle.

Table 8 – Protocol used for the slow cycle life tests.

Cycling Part	Step Number	Step Name	Step Time	Voltage Limit [V]	Current Density [mA/g]	Cut-off Current [mA]	Time Record [s]
Insulation Testing	1	-					
Formation Cycles	2	Rest	12 hr	-	-	-	30 sec
	3	CC Charge	-	1.75	20	-	10 sec
	4	CV Charge	3 hr	1.75	20	0.01	10 sec
	5	Rest	10 min	-	-	-	30 sec
	6	CC Discharge	-	1.15	20	-	10 sec
	7	CC DCIR Discharge	3 sec	-	60	-	0.1 sec
	8	Cycle	Start Step: 3 Cycle Count: 2				
Cycle Life Tests	9	Rest	10 min	-	-	-	30 sec
	10	CC Charge	-	1.75	10	-	10 sec

	11	CV Charge	3 hr	1.75	10	0.01	10 sec
	12	Rest	10 min	-	-	-	30 sec
	13	CC Discharge	-	1.15	10	-	10 sec
	14	CC DCIR Discharge	3 sec	-	60	-	0.1 sec
	15	Cycle	Start Step: 9 Cycle Count: 83				
End	28	-					

In Figure 44, the graphs obtained for both cells representing the discharge capacity and internal resistance of each cycle are shown. When comparing the data related to each cell, it can be clearly observed that cell P2398 presents a strange behaviour. Not only does this cell present much higher values for internal resistance but, for both discharge capacity and DCIR, the datapoints seem to fluctuate substantially. This high dispersion could be explained by a malfunction either inside the cell or from the channel used for testing, and so the data related to cell P2398 was not analysed any further.

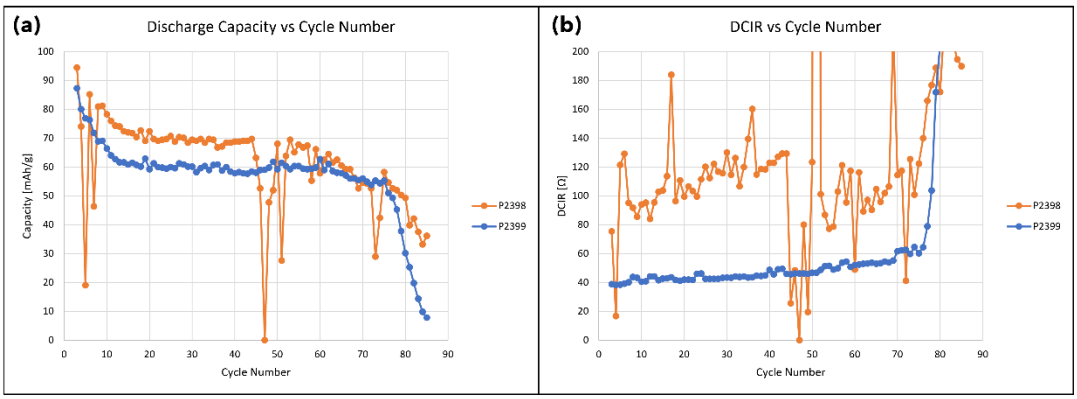

Figure 44 - Discharge capacity and DCIR as a function of the cycle number for both cells.

Nevertheless, regarding the datapoints associated with cell P2399, a very stable behaviour is seen for both discharge capacity and internal resistance – almost constant values are observed for the 2 parameters for the majority of the cycling. However, as can also be read from the capacity retention data presented in Figure 45 (a), when reaching approximately cycle 75, the cell begins to die, increasing quickly and largely its internal resistance and consequently decreasing its discharge capacity. Considering that each slow cycle takes a substantial amount of time (around 15 hours), it is worth mentioning that these cells had been cycling for a long

time (in total around 53 days). Therefore, since the longer the cells run the more probable it is for them to be affected by external factors, such as electrolyte drying and coating delamination, it was concluded that these extrinsic aspects were the reason for the ending of the stable behaviour of the cell. This conclusion can also be sustained by the strange readings seen in the cycling profile presented in Figure 45 (b) – the negative voltage values read are associated with the delamination of the coating from the current collector and the dried separator.

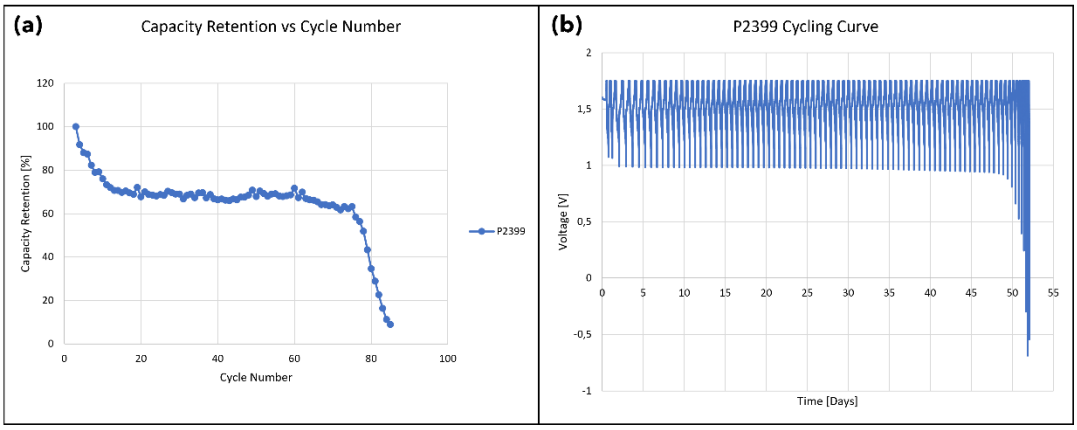

Figure 45 – Capacity retention as a function of cycle number and cycling curve of cell P2399.

Nevertheless, as was observed previously for 2 cells from the room temperature dataset, this result is another indication that a very stable cell can in fact be obtained, with its stable period only coming to an end due to factors external to the electrochemistry mechanisms happening in the cell. The drying of the electrolyte inside the cell (caused mainly due to poor case sealing) and the delamination of the coating are considered the most important aspects that prevent the cell from maintaining a good constant behaviour.

Lastly, it is worth mentioning that for every cell that seemed to present these 2 factors in the end of their cycling life, a post-mortem analysis was performed by opening their cases. As a result, it was seen that all of them showed a dried separator and the cathodic coating disconnected from the current collector and stuck in the separator. As an example, a picture from the post-mortem of cell P2399 is shown in Figure 46.

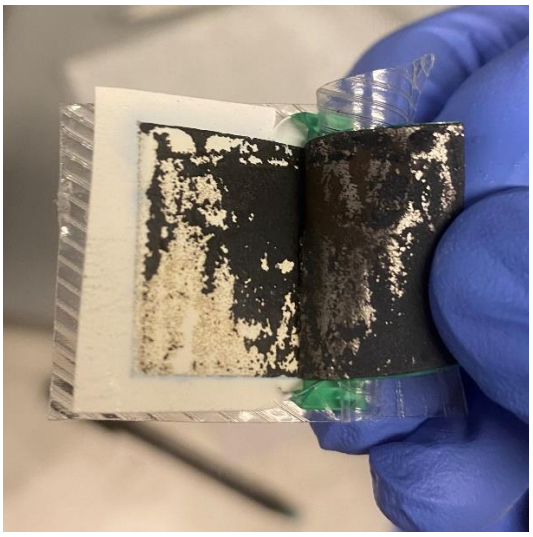

Figure 46 – Post-mortem analysis of cell P2399 – the cathodic coating is delaminated from the current collector and stuck into the separator.

7.8 Conclusions from the Cycle Life Tests

The main aim of the cycle life tests was to understand how the cells, which had been previously formed and some self-discharged, behaved when submitted to a large number of cycles. Furthermore, by trying to find correlations between the formation cycle parameters and the good or bad behaviour of the cells, a grading and quality control system could be conceived and implemented in the manufacturing process.

When analysing the results, the first conclusion observed was that, for each dataset studied, the correlations between the aforementioned parameters and the definition of the cells as good or bad varied when the capacity retention threshold chosen for the grading changed. The challenge is that in each dataset (temperature condition), the cells were aged in a different way and therefore a global threshold cannot be well defined. Moreover, between different datasets, correlations with distinct parameters appeared and no variable showed a strong correlation for every threshold or every dataset. Lastly, the situation only worsened when the datasets were combined and studied together, with no parameter showing any correlation with the grading of the cells.

For this reason, no strong conclusions could be drawn from the correlations analysis. This lack of desired results could be associated with an insufficient number of datapoints used for the analysis. For the room temperature and 25°C datasets, and for the 5°C dataset, only 6 and 8 datapoints, respectively, were used in the analysis. However, by greatly increasing the number of cells studied, new and stronger correlations could appear, leading to more reliable conclusions.

The major challenge seen in this experiment is that there is no way of knowing how and when the cells die over time. For example, if the electrolyte is drying or the coating delaminating from the foil, the performance of the cell will certainly get worse, thus influencing the grading of the cell as good or bad. Furthermore, these 2

extrinsic factors are not visible in the formation cycles, normally happening after several days of cycling. It is noteworthy that the delamination of the coating seen in the pouch cells is a direct consequence of electrolyte drying. Therefore, no quality control step after cell formation could directly predict and prevent coating delamination, since, as observed, the electrolyte starts to dry unpredictably after the cell has been cycled several times due to a poor pouch cell sealing, which, unfortunately, cannot be detected in advance by any setup in Enerpoly AB facility. It must therefore be suggested that, in future quality control methodology, a careful verification of case sealing should be included, in order to prevent electrolyte drying, which significantly influences the cycling stability of the cells.

Nevertheless, some conclusions can be taken from this procedure and analysis. On one hand, cells P2330 and P2337 from the room temperature dataset and cell P2399 from the slow cycle life tests show that it is possible to assemble a very stable cell, whose approximately constant behaviour only ends when influenced by the previously mentioned external factors. However, even though this can be seen as a positive conclusion, since it shows that with a proper sealing and coating a highly durable and stable cell can be achieved, it poses an important question about the analysis: this could mean that, when grading the cells as good or bad, a wrong judgement is being made by justifying the capacity fading with cell degradation, when in fact could only be related to external factors. In order to evaluate this hypothesis, a higher number of cells should be tested, to evaluate the differences in behaviour between stable cells.

Finally, the most important aspect to notice from the analysis is that every time the datapoints from a specific cell were discarded, the decision was based on either a fast rise of the internal resistance (most probably associated with electrolyte drying) or the initial gravimetric capacity being too low (most probably related to uneven coating or delamination). Therefore, this could indicate that a good quality control system for the manufacturing process, checking good cell casing, good coating adhesion, low internal resistance, high gravimetric capacity, and no short circuits from the stack, could be essential and sufficient to determine the system's performance and discard faulty and malfunctioning cells.

Having reached this conclusion, a possible way of performing cell grading could be focusing on two aspects: (1) the quality control tests on the dry cell – checking individual components of the cell, and ensuring good case sealing, no short circuits, and good coating quality – and (2) on the wet cell – running several tests focused on checking if the internal resistance is still high after electrolyte filling, if the gravimetric capacity is high after the formation cycles, and performing a DCIR again after the cell is formed. By following this protocol, the dry cell quality checks would ensure that no electrolyte drying or poor coating could influence the stable behaviour of the cell, and the wet cell quality checks would guarantee that malfunctioning cells are discarded and recycled before being integrated into a pack. To conclude, if the cells can pass all these quality control checking standards, there is a high chance that a high quality stable system is achieved, as the cells seen in the room temperature dataset.

8 Summary and Conclusions

The study performed for this thesis aimed to contribute for the literature regarding grading and quality control of zinc-ion battery cells. For this purpose, several pouch cells were assembled and submitted to various tests in order to understand and relate their formation, self-discharge, and cycle life behaviour.

In order to comprehend if the intended protocol was applicable for the studied cells, providing the desired data for the future analysis, primary testing was carried out in 2 cells. Even though these validated the methodology, an unexpected 2-plateau self-discharge curve was observed for both cells. Consequently, an extensive study was completed to verify the reliability of these results, since they contrasted with what was found in the literature. It was concluded that the reason behind the 2-plateau self-discharge curves was related to a malfunctioning in the company's cycler, which was instantaneously leaking current from all channels into the terminals of the cells. Nevertheless, since momentaneous small current leakages do not affect the behaviour of the cells unless when at rest, the cycler continued to be used for the rest of the testing.

As part of the aforementioned study, distinct cells were formed using a different number of formation cycles. Therefore, a study was also performed to not only find correlations between the so-called formation cycle parameters but to understand how many formation cycles should be used in the future analysis. In conclusion, it was seen that these formation cycle parameters and the charge-discharge formation cycle curves started to tend to approximately constant values and shape, respectively, from the second cycle forward, and so 2 formation cycles were chosen for the rest of the analysis.

After having established the protocol for the desired testing, the self-discharge behaviour of zinc-ion cells was analysed. In order to try to avoid the previously mentioned problems related to the cycler, 3-day self-discharge tests were performed at the company's cycler, and 2-week tests at a non-faulty one. From the latter, it was established that a 1-plateau self-discharge curve was in fact the correct shape and behaviour for zinc-ion cells. However, when comparing with the 1-plateau data acquired, the voltage drop obtained (for the first 3 days) was significantly higher than the 3-day one. Considering that the cells submitted to the 3-day resting period had already gone through a longer protocol before, this result was contradictory. Therefore, it was concluded that, even though the influence of the cycler was reduced by decreasing the resting time (avoiding a 2-plateau curve), these results could once again be justified by malfunctioning in the cycler causing current leakages. For this reason, since no self-discharge parameters could be assumed as reliable, no further analysis was performed using this data.

As grading and quality control intend to distinguish good from bad cells, cycle life tests were performed to analyse the behaviour of zinc-ion cells for a longer period of cycling time. 3 different datasets were submitted to these tests at 3 distinct temperatures – room temperature, 25°C, and 5°C. Having collected the datapoints for every cycle, the cells which presented strange behaviours were discarded from the analysis, and the rest divided into good or bad by defining capacity retention

thresholds for the last cycle of the protocol. Afterwards, correlations were investigated between the formation cycle parameters and the good or bad definition of the cells for each threshold.

In summary, even though some formation cycle parameters displayed strong correlations for specific datasets and thresholds, no variable exhibited a strong correlation for every threshold within a dataset or between datasets. Moreover, once datapoints of 2 or even all datasets were combined, no parameter presented any strong correlation. For these reasons, no conclusions can be drawn connecting the parameters read in the formation cycles with the future behaviour of the cells. Therefore, it is impossible to state that, by only examining a specific formation cycle parameter, the good or bad behaviour of the cell can be predicted. Nevertheless, the lack of strong correlations found could be associated with the low number of datapoints used for the analysis. By performing the tests in a higher number of cells, stronger or even newer correlations could be found.

However, conclusions were drawn from the cycle life tests concerning the grading and quality control protocol. From the cells tested, not only 3 presented a very stable constant behaviour throughout the whole cycling, but the ones that were eventually discarded, due to malfunction, showed always either a fast rise of the internal resistance with time or a low gravimetric capacity after formation. These two behaviours are directly associated with external factors observed, specifically to electrolyte drying and delamination of coating. For these reasons, a possible suggested good method for performing cell grading and quality control could be to perform tests to check case sealing, absence of short circuits, and coating quality on the dry cell, and internal resistance measurements after electrolyte filling, capacity determination and DCIR after cell formation on the wet cell. If this protocol is followed, the combination of the dry cell with the wet cell quality checks ensures that not only no electrolyte drying or poor coating influence the stable behaviour of the cell but also that malfunctioning cells are discarded and recycled before being integrated in a pack.

In the introduction of this thesis, 4 research questions were posed to help guide and advance the research conducted. As a final remark, the answers to these questions summarize the conclusions presented above. It can be concluded that the tests used in the more mature lithium-ion battery industry are sufficient to perform the grading and quality control of zinc-ion battery cells. Moreover, not all types of tests mentioned in the introduction are necessary, with the suggested grading and quality control protocol only utilizing internal resistance and discharge capacity measurements. Regarding the relation between formation and self-discharge parameters and good or bad performance of the cells, unfortunately no strong connection was found, which leads to the conclusion that none of these variables could predict the future behaviour of zinc-ion cells in this current study. However, as mentioned, increasing the number of datapoints could be necessary for the appearance of stronger correlations. Finally, external factors, as electrolyte drying or delamination of coating, were found to have a crucial impact in the behaviour of the cells, contributing immensely to their capacity fading, and therefore the proposed quality control protocol aimed to diminish their influence.

9 Future Research

In this section, some recommendations and ideas for future research and analysis in this topic are presented.

On one hand, increasing the number of tested cells for the cycle life tests could be interesting and critical to find stronger correlations between the formation cycle parameters and the good or bad performance of the cells. This could lead to stronger conclusions, enabling the prediction of the future behaviour of a zinc-ion battery cell by only the measurement of a single formation variable. Furthermore, by employing a non-faulty cycler, reliable self-discharge parameters could be obtained and also utilized to find such correlations, enabling the integration of a self-discharge protocol into the grading and quality control process.

On the other hand, as external factors contributed significantly to the capacity decrease of several cells, it is important to notice that further research has to be performed to fully understand what is really causing the cells to die. Since very stable cells were also seen, it could be possible that a wrong assumption is being made relating capacity fading with cell degradation, when the latter is only due to electrolyte drying or coating delamination. By studying cells with better and verifiable case sealing and coating adhesion and evenness, the factors influencing capacity fading could be better understood.

Lastly, as a final step, the studies performed throughout this thesis for pouch cells must be reproduced for prismatic cells, since these will be the ones composing the battery packs. These tests will enable the identification of internal resistance and capacity limits and thresholds crucial for the grading and quality control process.

References

[1] Maeve Campbell, “We’re facing a lithium battery crisis: What are the alternatives?,” *euronews.green*, Feb. 09, 2022.

[2] W. Lu and X. Li, “Progress and Perspectives of Flow Battery Technologies,” *Electrochemical Energy Reviews*, vol. 2, Jun. 2019, doi: 10.1007/s41918-019-00047-1.

[3] J.-M. Tarascon and M. Armand, “Issues and challenges facing rechargeable lithium batteries,” *Nature*, vol. 414, no. 6861, pp. 359 – 367, 2001, doi: 10.1038/35104644.

[4] Peter Hannah, “How can you manage price volatility in the lithium market?,” *Fastmarkets*, Jul. 12, 2022.

[5] Govind Bhatada, “Visualizing China’s Dominance in Battery Manufacturing (2022-2027P),” *Visual Capitalist*, Jan. 19, 2023.

[6] Veronika Henze, “Lithium-ion Battery Pack Prices Rise for First Time to an Average of $151/kWh,” *BloombergNEF*, Dec. 06, 2022.

[7] Frik Els, “And the winner for most volatile commodity this decade goes to… lithium,” *Mining.com*, Jan. 12, 2023.

[8] N. Wang *et al.*, “A review of zinc-based battery from alkaline to acid,” *Materials Today Advances*, vol. 11. Elsevier Ltd, Sep. 01, 2021. doi: 10.1016/j.mtadv.2021.100149.

[9] M. Al-Amin, S. Islam, S. U. A. Shibly, and S. Iffat, “Comparative Review on the Aqueous Zinc-Ion Batteries (AZIBs) and Flexible Zinc-Ion Batteries (FZIBs),” *Nanomaterials*, vol. 12, no. 22. MDPI, Nov. 01, 2022. doi: 10.3390/nano12223997.

[10] Q.-N. Zhu *et al.*, “Challenges and strategies for ultrafast aqueous zinc-ion batteries,” *Rare Metals*, vol. 40, no. 2, pp. 309–328, 2021, doi: 10.1007/s12598-020-01588-x.

[11] U. Siamionau *et al.*, “Rechargeable zinc-ion batteries with manganese dioxide cathode: How critical is choice of manganese dioxide polymorphs in aqueous solutions?,” *J Power Sources*, vol. 523, Mar. 2022, doi: 10.1016/j.jpowsour.2022.231023.

[12] F. Wang *et al.*, “Highly reversible zinc metal anode for aqueous batteries,” *Nat Mater*, vol. 17, no. 6, pp. 543–549, Jun. 2018, doi: 10.1038/s41563-018-0063-z.

[13] D. Kundu, B. D. Adams, V. Duffort, S. H. Vajargah, and L. F. Nazar, “A high-capacity and long-life aqueous rechargeable zinc battery using a metal oxide intercalation cathode,” *Nat Energy*, vol. 1, no. 10, p. 16119, 2016, doi: 10.1038/nenergy.2016.119.

[14] M. Garside, “Zinc Metal Production Volume worldwide 2005-2022,” *Statista*, May 22, 2023.

[15] M. Garside, “Global Lithium Mine Production 2010-2022,” *Statista*, Mar. 21, 2023.

[16] T. B. Reddy, *Linden’s Handbook of Batteries, Fourth Edition*, Fourth Edition. New York: McGraw-Hill Education, 2011. [Online]. Available: https://www.accessengineeringlibrary.com/content/book/9780071624213

[17] B. Sambandam *et al.*, “An analysis of the electrochemical mechanism of manganese oxides in aqueous zinc batteries,” *Chem*, vol. 8, no. 4. Elsevier Inc., pp. 924–946, Apr. 14, 2022. doi: 10.1016/j.chempr.2022.03.019.

[18] C. Li *et al.*, “Spatially homogeneous copper foam as surface dendrite-free host for zinc metal anode,” *Chemical Engineering Journal*, vol. 379, p. 122248, 2020, doi: https://doi.org/10.1016/j.cej.2019.122248.

[19] W. Sun *et al.*, “Zn/MnO2 Battery Chemistry with H+ and Zn2+ Coinsertion,” *J Am Chem Soc*, vol. 139, no. 29, pp. 9775–9778, Jul. 2017, doi: 10.1021/jacs.7b04471.

[20] Enerpoly AB, “Enerpoly AB,” *https://www.enerpoly.com/*.

[21] Melasta Battery, “Lithium Battery Cell Grading System - How to distinguish Grade A, B and C Cells?,” *https://www.youtube.com/watch?v=6hv4kCq1X48*, Jun. 28, 2022.

[22] E. Kartini *et al.*, “Grading of Lithium Ion Battery Module for Public street lighting,” in *IOP Conference Series: Materials Science and Engineering*, Institute of Physics Publishing, Nov. 2019. doi: 10.1088/1757-899X/553/1/012065.

[23] H. Pan *et al.*, “Reversible aqueous zinc/manganese oxide energy storage from conversion reactions,” *Nat Energy*, vol. 1, Mar. 2016, doi: 10.1038/nenergy.2016.39.

[24] H. Glatz, E. Tervoort, and D. Kundu, “Unveiling Critical Insight into the Zn Metal Anode Cyclability in Mildly Acidic Aqueous Electrolytes: Implications for Aqueous Zinc Batteries,” *ACS Appl Mater Interfaces*, vol. 12, no. 3, pp. 3522–3530, 2020, doi: 10.1021/acsami.9b16125.

[25] C. Chachet, B. Saidani, and R. Wiart, “The Behavior of Zinc Electrode in Alkaline Electrolytes,” *J Electrochem Soc*, 1992.

[26] M. Chamoun, W. R. Brant, C. W. Tai, G. Karlsson, and D. Noréus, “Rechargeability of aqueous sulfate Zn/MnO2 batteries enhanced by accessible Mn2+ ions,” *Energy Storage Mater*, vol. 15, pp. 351–360, Nov. 2018, doi: 10.1016/j.ensm.2018.06.019.

[27] J. Lee, J. B. Ju, W. Il Cho, B. W. Cho, and S. H. Oh, “Todorokite-type MnO2 as a zinc-ion intercalating material,” *Electrochim Acta*, vol. 112, pp. 138–143, 2013, doi: 10.1016/j.electacta.2013.08.136.

[28] B. Lee, C. S. Yoon, H. R. Lee, K. Y. Chung, B. W. Cho, and S. H. Oh, "Electrochemically-induced reversible transition from the tunneled to layered polymorphs of manganese dioxide," *Sci Rep*, vol. 4, Aug. 2014, doi: 10.1038/srep06066.

[29] Y. Qiu *et al.*, "Vanadium Oxide-Based Cathode Materials for Aqueous Zinc-Ion Batteries: Energy Storage Mechanism and Design Strategy," *Inorganics (Basel)*, vol. 11, no. 3, p. 118, Mar. 2023, doi: 10.3390/inorganics11030118.

[30] P. Oberholzer, E. Tervoort, A. Bouzid, A. Pasquarello, and D. Kundu, "Oxide vs. Non-oxide Cathode Materials for Aqueous Zn Batteries: An Insight into the Charge Storage Mechanism and Consequences Thereof," 2019.

[31] A. Omar, O. Bahdad, J. Bravo-Suarez, and L. Liu, "Characterization of the Electron Transfer Reaction Mechanism of TiOSO4 and MnSO4 in Sulfuric Acid Solution," 2020.

[32] J. Yang *et al.*, "Unravelling the Mechanism of Rechargeable Aqueous Zn–MnO2 Batteries: Implementation of Charging Process by Electrodeposition of MnO2," *ChemSusChem*, vol. 13, no. 16, pp. 4103–4110, Aug. 2020, doi: 10.1002/cssc.202001216.

[33] P. Vanysek, *CRC Handbook of Chemistry and Physics*, vol. 8. Marcel Dekker, 2023.

[34] M. Song, H. Tan, D. Chao, and H. J. Fan, "Recent Advances in Zn-Ion Batteries," *Adv Funct Mater*, vol. 28, no. 41, p. 1802564, 2018, doi: https://doi.org/10.1002/adfm.201802564.

[35] B. Hertzberg *et al.*, "The effect of multiple cation electrolyte mixtures on rechargeable Zn-MnO2 alkaline batteries," *Chemistry of Materials*, vol. 28, Mar. 2016, doi: 10.1021/acs.chemmater.6b00232.

[36] S. H. Kim and M. Oh, "Degradation mechanism of layered MnO2 cathodes in Zn/ZnSO4/MnO2 rechargeable cells," 1998.

[37] R. C. Massé and J. B. Gerken, "Assembly of a robust and economical MnO2-based reference electrode," *J Chem Educ*, vol. 92, no. 1, pp. 110–115, Jan. 2015, doi: 10.1021/ed500587a.

[38] M. H. Alfaruqi *et al.*, "Structural transformation and electrochemical study of layered MnO2 in rechargeable aqueous zinc-ion battery," *Electrochim Acta*, vol. 276, pp. 1–11, Jun. 2018, doi: 10.1016/j.electacta.2018.04.139.

[39] Elizabeth Makley, "Grade A Solutions for Battery Grading," *Tektronix*, Jun. 29, 2022.

[40] WinAck, "Benefits of High-precision EV Battery Formation and Grading System," *https://www.winackbattery.com/news/High-precision-EV-Battery-Formation-and-Grading-System.html*, Aug. 27, 2020.

[41] M. Westermeier, G. Reinhart, and T. Zeilinger, "Method for quality parameter identification and classification in battery cell production quality planning of complex production chains for battery cells," in *2013 3rd*

International Electric Drives Production Conference, EDPC 2013 - Proceedings, IEEE Computer Society, 2013. doi: 10.1109/EDPC.2013.6689742.

[42] Seplos Technology, "How to Distinguish Grade A and Grade B Cells - LiFePO4 Prismatic cell," *https://www.youtube.com/watch?v=vJlL-oX70WM*. Dec. 09, 2019.

[43] TÜV SÜD, "Battery Safety and Abuse Testing," *https://www.tuvsud.com/en/industries/mobility-and-automotive/automotive-and-oem/automotive-testing-solutions/battery-testing/battery-safety-and-abuse-testing*.

[44] A. Barai *et al.*, "A comparison of methodologies for the non-invasive characterisation of commercial Li-ion cells," *Progress in Energy and Combustion Science*, vol. 72. Elsevier Ltd, pp. 1–31, May 01, 2019. doi: 10.1016/j.pecs.2019.01.001.

[45] A. Kirchev, "Battery Management and Battery Diagnostics," in *Electrochemical Energy Storage for Renewable Sources and Grid Balancing*, Elsevier Inc., 2015, pp. 411–435. doi: 10.1016/B978-0-444-62616-5.00020-6.

[46] Battery University, "What Is C-rate?," 2021. https://batteryuniversity.com/article/bu-402-what-is-c-rate (accessed Apr. 04, 2023).

[47] A. Barai, "Improvement of Consistency, Accuracy and Interpretation of Characterisation Test Techniques for Li-ion Battery cells for Automotive Application," 2015. [Online]. Available: http://go.warwick.ac.uk/wraphttp://go.warwick.ac.uk/wrap/77676

[48] A. Barai, K. Uddin, W. D. Widanalage, A. McGordon, and P. Jennings, "The effect of average cycling current on total energy of lithium-ion batteries for electric vehicles," *J Power Sources*, vol. 303, pp. 81–85, Jan. 2016, doi: 10.1016/j.jpowsour.2015.10.095.

[49] R. Zhang *et al.*, "Study on the characteristics of a high capacity nickel manganese cobalt oxide (NMC) lithium-ion battery-an experimental investigation," *Energies (Basel)*, vol. 11, no. 9, Sep. 2018, doi: 10.3390/en11092275.

[50] M. F. Robbins, "Open Circuit and Short Circuit," *Ultimate Electronics Book*, 2021. https://ultimateelectronicsbook.com/open-circuit-and-short-circuit/ (accessed Apr. 04, 2023).

[51] C. R. Birkl, E. McTurk, M. R. Roberts, P. G. Bruce, and D. A. Howey, "A Parametric Open Circuit Voltage Model for Lithium Ion Batteries," *J Electrochem Soc*, vol. 162, no. 12, pp. A2271–A2280, Sep. 2015, doi: 10.1149/2.0331512JES.

[52] Battery Design, “Open Circuit Voltage,” 2023. https://www.batterydesign.net/electrical/open-circuit-voltage/ (accessed Apr. 04, 2023).

[53] E. Keszei, *Chemical Thermodynamics - An Introduction*. 2012.

[54] A. Farmann and D. U. Sauer, “A study on the dependency of the open-circuit voltage on temperature and actual aging state of lithium-ion batteries,” *J Power Sources*, vol. 347, pp. 1–13, 2017, doi: 10.1016/j.jpowsour.2017.01.098.

[55] K. Uddin, A. Picarelli, C. Lyness, N. Taylor, and J. Marco, “An acausal Li-ion battery pack model for automotive applications,” *Energies (Basel)*, vol. 7, no. 9, pp. 5675–5700, 2014, doi: 10.3390/en7095675.

[56] W. Waag, S. Käbitz, and D. U. Sauer, “Experimental investigation of the lithium-ion battery impedance characteristic at various conditions and aging states and its influence on the application,” *Appl Energy*, vol. 102, pp. 885–897, 2013, doi: 10.1016/j.apenergy.2012.09.030.

[57] X. Hu, S. Li, and H. Peng, “A comparative study of equivalent circuit models for Li-ion batteries,” *J Power Sources*, vol. 198, pp. 359–367, Jan. 2012, doi: 10.1016/j.jpowsour.2011.10.013.

[58] A. Łebkowski, “Temperature, Overcharge and Short-Circuit Studies of Batteries used in Electric Vehicles,” *Przeglad Elektrotechniczny*, vol. 93, no. 5, pp. 67–73, 2017, doi: 10.15199/48.2017.05.13.

[59] K. Gaouzi, H. El Fadil, A. Rachid, A. Lassioui, Z. El Idrissi, and F. Giri, “Sampled-Data Observer for Estimating the State of Charge, State of Health, and Temperature of Batteries,” *Electric Power Components and Systems*, vol. 48, no. 19–20, pp. 2168–2180, 2021, doi: 10.1080/15325008.2021.1913262.

[60] J. Kowal, “Spatially-resolved impedance of nonlinear inhomogeneous devices using the example of lead-acid batteries,” Technische Hochschule Aachen, 2010.

[61] H. Wenzl, “Self-Discharge Definitions and Terms,” 2009.

[62] B. Zollo, “Measure Self-Discharge Using OCV on Lithium-Ion Cells,” *Electronic Design*, Jul. 30, 2019. https://www.electronicdesign.com/technologies/test-measurement/article/21808344/keysight-technologies-measure-selfdischarge-using-ocv-on-lithiumion-cells (accessed Apr. 05, 2023).

[63] D. Theuerkauf and L. Swan, “Characteristics of Open Circuit Voltage Relaxation in Lithium-Ion Batteries for the Purpose of State of Charge and State of Health Analysis,” *Batteries*, vol. 8, no. 8, Aug. 2022, doi: 10.3390/batteries8080077.

[64] K. Alam Khan, M. Afzol Hossain, M. Afzol Hossain, A. K. M Obaydullah, and M. Wadud, “PKL Electrochemical Cell and the Peukert’s Law,” 2018. [Online]. Available: https://www.researchgate.net/publication/324792341

[65] M. Haque *et al.*, “Identification of self-discharge mechanisms of ionic liquid electrolyte based supercapacitor under high-temperature operation,” *J Power Sources*, vol. 485, Feb. 2021, doi: 10.1016/j.jpowsour.2020.229328.

[66] Battery University, “What does Elevated Self-discharge Do?,” Nov. 02, 2021. https://batteryuniversity.com/article/bu-802b-what-does-elevated-self-discharge-do (accessed Apr. 05, 2023).

[67] Batteries Plus, “How Do Battery Charging Cycles Work?,” Nov. 16, 2021. https://www.batteriesplus.com/blog/power/battery-discharge-cycle (accessed Apr. 06, 2023).

[68] M. Qadrdan, N. Jenkins, and J. Wu, “Smart Grid and Energy Storage,” in *McEvoy’s Handbook of Photovoltaics (Third Edition)*, S. A. Kalogirou, Ed., Third Edition.Academic Press, 2018, pp. 915–928. doi: https://doi.org/10.1016/B978-0-12-809921-6.00025-2.

[69] N. Maluf, “What Happens After 80%?,” *Qnovo*, Oct. 27, 2014.

[70] A. Solntsev *et al.*, “Influence of temperature on the performance and life cycle of storage batteries,” in *Transportation Research Procedia*, Elsevier B.V., 2021, pp. 652–659. doi: 10.1016/j.trpro.2021.09.096.

[71] Electropaedia, “Battery Life (and Death),” 2005. https://www.mpoweruk.com/life.htm#changes (accessed Apr. 06, 2023).

[72] S. S. Choi and H. S. Lim, “Factors that affect cycle-life and possible degradation mechanisms of a Li-ion cell based on LiCoO 2,” *J Power Sources*, vol. 111, pp. 130–136, 2002.

[73] W. Waag and D. U. Sauer, “Secondary Batteries - Lead Acid Systems - State-of-Charge/Health,” *Encyclopedia of Electrochemical Power Sources*, pp. 793–804, Jan. 2009, doi: 10.1016/B978-044452745-5.00149-0.

[74] J. Daniel-Ivad, “Zinc-Manganese,” Richmond Hill, ON, Canada, 2009.

[75] HIOKI, “Lithium-ion Battery Insulation Resistance Testing,” *HIOKI*, 2023.

[76] R. Bollini, “Understanding memory effect in Lithium-ion batteries,” *EVReporter*, Jul. 25, 2022. https://evreporter.com/understanding-memory-effect-in-lithium-ion-batteries/ (accessed Apr. 18, 2023).

[77] K. Zhao *et al.*, “Ultrathin Surface Coating Enables Stabilized Zinc Metal Anode,” *Adv Mater Interfaces*, vol. 5, no. 16, p. 1800848, Aug. 2018, doi: 10.1002/ADMI.201800848.

[78] D. Wang, H. Liu, D. Lv, C. Wang, J. Yang, and Y. Qian, “Rational Screening of Artificial Solid Electrolyte Interphases on Zn for Ultrahigh-Rate and Long-Life Aqueous Batteries,” *Advanced Materials*, vol. 35, no. 2, p. 2207908, Jan. 2023, doi: 10.1002/ADMA.202207908.

[79] A. Konarov, “Self-discharge of Rechargeable Hybrid Aqueous Battery,” University of Waterloo, Waterloo, Ontario, 2014.

[80] R. Fang, P. Dong, H. Ge, J. Fu, Z. Li, and J. Zhang, “Capacity plunge of lithium-ion batteries induced by electrolyte drying-out: Experimental and Modeling Study,” *J Energy Storage*, vol. 42, Oct. 2021, doi: 10.1016/j.est.2021.103013.

[81] Jason Fernando, “R-Squared: Definition, Calculation Formula, Uses, and Limitations,” *Investopedia*, Apr. 08, 2023.

[82] Corporate Finance Institute, “Correlation Matrix,” Aug. 07, 2019.